Marine Geology 361 (2015) 79–95

Contents lists available at ScienceDirect

Marine Geology

journal homepage: www.elsevier.com/locate/margeo

The Al-Borani submarine landslide and associated tsunami. A modelling approach ☆

J. Macías [a,*], J.T. Vázquez [b], L.M. Fernández-Salas [c], J.M. González-Vida [d], P. Bárcenas [a], M.J. Castro [a], V. Díaz-del-Río [b], B. Alonso [e]

[a] Departamento de Análisis Matemático, Facultad de Ciencias, Universidad de Málaga, Campus de Teatinos s/n, 29080 Málaga, Spain
[b] Instituto Español de Oceanografía, Centro Oceanográfico de Málaga, Puerto Pesquero s/n, 29640 Fuengirola, Spain
[c] Instituto Español de Oceanografía, Centro Oceanográfico de Cádiz, Puerto Pesquero, Muelle de Levante s/n, 11006 Cádiz, Spain
[d] Departamento de Matemática Aplicada, Escuela Politécnica Superior, Universidad de Málaga, Campus de Teatinos s/n, 29071 Málaga, Spain
[e] Instituto de Ciencias del Mar, CSIC, Passeig Maritim, 37–49, 08003, Barcelona, Spain

ARTICLE INFO

Article history:
Received 7 February 2014
Received in revised form 27 December 2014
Accepted 29 December 2014
Available online 7 January 2015

Keywords:
Submarine landslide
Palaeo-tsunami
Alboran sea ridge
Al-Borani Canyon-Fan
Numerical simulation
HySEA model

ABSTRACT

The key goals to studying submarine landslides and associated tsunamis are to better assess the magnitude information of palaeo-tsunamis and to contribute to assessing future tsunami risks. The numerical modelling of submarine landslides and the tsunamis thus generated comprises important interdisciplinary research that requires knowledge of both geology and numerical modelling. Models are capable of delineating the time evolution of tsunami hydrodynamics, sediment transport, and the resulting morphological changes associated with deposition. To advance towards the ultimate goal of improved tsunami risk assessment, modellers and geologists need to develop an in-depth mutual understanding of the advantages, limitations, and uncertainties in both numerical modelling and geological records. In this work, seafloor features related to former submarine landslides in the Alboran Sea basin have been identified through multibeam bathymetry data and high- to very high-resolution seismic profiles. The mathematical modelling and hindcasting have been performed through numerical simulation of a hypothetical submarine landslide and the associated tsunami that could have originated one of the submarine landslides identified. This system, on the southern Alboran Ridge slope, is currently reworked by turbidite processes, forming a submarine canyon-sedimentary fan system known as the Al-Borani System. The HySEA numerical model simulates the submarine landslide triggering the tsunami and the water mass evolution, wave propagation, and the final penetration of the tsunami waves onto the coast, reproducing initial and subsequent tsunami wave impacts by means of a single coupled numerical model. This numerical model allows an analysis of the influence of basin morphology on the tsunami propagation features, such as shape and propagation patterns, speed or wave amplitude and, finally, its impact on the coast (in this case South Iberia and North Africa). This model can also be used as a prediction tool for the simulation of potential landslides, many of which generate tsunamis. Monitoring of critical areas, where landslides are more probable, and modelling their consequences will allow a choice of the appropriate mitigation strategies. Therefore, monitoring and modelling are areas of key scientific and socio-economic interests.

1. Introduction

Tsunami wave generation is a geological hazard that can have a severe impact on society. Coastal areas are not only the most populated regions of the planet, but also where economic activity clusters. Tourism is a significant activity on the South Iberian coastline and an emergent one on the North African coastline (growing continuously over the last decade) (Fig. 1).

To evaluate the tsunami risk in a region, it is necessary first to consider the most probable tsunamigenic sources. The two major geological mechanisms generating tsunamis that have to be considered are seismic–tectonic activity and sedimentary instability processes that generate submarine landslides, in particular, subaerial or submarine landslides affecting the seafloor surface. In the Alboran basin, the study of tsunamis triggered by seismic–tectonic activity has been considered by several authors in recent years (González et al., 2010; Álvarez-Gómez et al., 2011a,b). As an example, Álvarez-Gómez et al. (2011a and b) deal with tsunami generation from both the tectonics and potential seismic sources in this marine region. They consider 12

☆ A five-step educational sketch summarizing the hypothesis, methodological process and results of this study can be found at: edanya.uma.es/menulandslides/109.

* Corresponding author. Tel.: +34 952132016.
E-mail addresses: jmacias@uma.es (J. Macías), juantomas.vazquez@ma.ieo.es (J.T. Vázquez), luismi.fernandez@cd.ieo.es (L.M. Fernández-Salas), jgv@uma.es (J.M. González-Vida), pbarcenas@uma.es (P. Bárcenas), mjcastro@uma.es (M.J. Castro), diazdelrio@ma.ieo.es (V. Díaz-del-Río), belen@icm.csic.es (B. Alonso).

http://dx.doi.org/10.1016/j.margeo.2014.12.006
0025-3227/

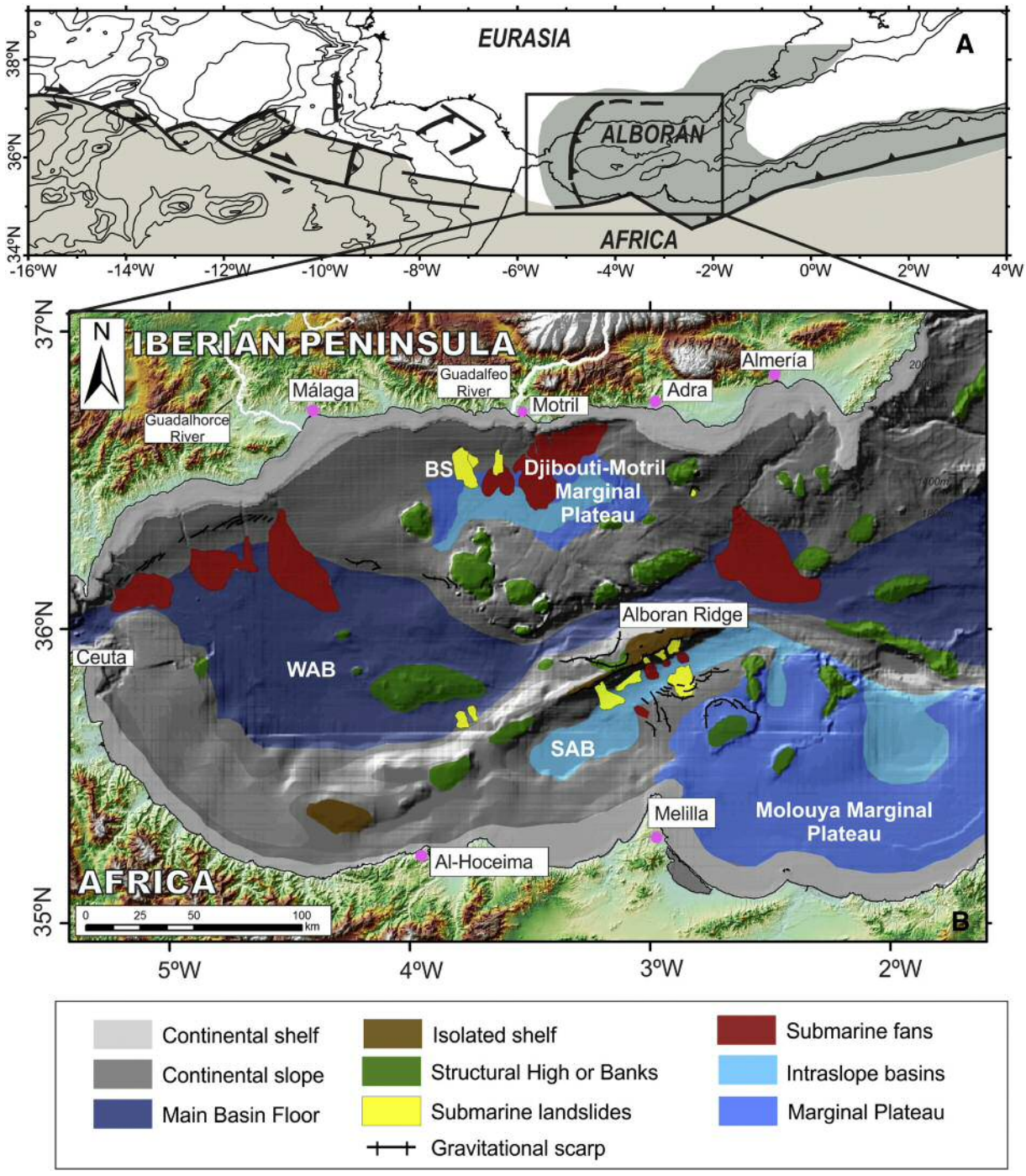

Fig. 1. (A) Plate-tectonic scheme of the Ibero–Maghrebian region (modified from Vázquez and Vegas, 2000). WAS: Western Alboran Subduction Zone. (B) Physiographic Map of the Alboran Sea basin plotted on a hillshade model. A compilation of multibeam bathymetry (40 × 40 m) has been used for the construction of this model and has been plotted on a general hillshade model based on ETOPO bathymetry (1000 × 1000 m). On land, a DTM model has been used based on the 1° × 1° files available from the 2000 Shuttle Radar Topography Mission, the resolution is about 90 m. BS: Baraza slide. SAB: South Alboran Basin, WAB: West Alboran basin.

probable tsunamigenic seismic sources from geological studies of the seafloor. Their research concludes that earthquakes located on the Alboran Ridge show the maximum potential to generate damaging tsunamis, with a maximum wave elevation on the coast exceeding 1.5 m.

The study of tsunamis triggered by submarine landslides has increased considerably in the last 20 years. Our expanded knowledge of the seafloor due to the development of exploration techniques has revealed numerous submarine landslides on the seafloor surface. The observation of these features has spurred the evaluation of the role that submarine landslides play as potential tsunami sources in order to assess the hazard and risk to which a given coastal region is exposed (Harbitz, 1992; Haugen et al., 2005; Løvholt et al., 2005; Harbitz et al., 2006; Masson et al., 2006; Tappin, 2010; Harbitz et al., 2014). The triggering of submarine landslides usually includes several factors such as high-amplitude sea-level changes, sediment overburden, storms, the presence of bubble gas within the sediments and

dissociation of gas hydrate, overstepping, and tectonics-related earthquakes (Locat and Lee, 2002). In the Alboran Sea, landslide mechanisms have not been considered so far, although several cases have been studied in the Western Mediterranean Sea. The 1979 Nice tsunami (France) is recognized as the only landslide-generated tsunami historically recorded on the coastline of the Western Mediterranean Sea, and it has been suggested that an increase in pore pressure related with the construction of Nice airport was the triggering mechanism of this submarine landslide (Dan et al., 2007). In the 2003 Balearic Island tsunami (Spain), submarine landslide processes on the Algerian continental margin related to the Boumerdès-Zemmouri earthquake have been proposed as the generating mechanism; however, the main triggering factor has been linked to the earthquake coseismic deformation offshore (Sahal et al., 2009; Cattaneo et al., 2012). Recently, Iglesias et al. (2012) proposed a numerical simulation and scenario for a potential tsunami generated by the Big'95 landslide (Lastras et al., 2005) and show wave amplitudes between 3 m to over 9 m on the coasts around the Gulf of Valencia. The important role of landslides as tsunami-generation mechanisms and the lack of simulation studies of these kinds of events in the Alboran Sea region have motivated our focus on this type of tsunamis in this area of the Mediterranean Sea.

The aim of this work is to provide indications on the tsunami hazard posed by submarine landslide failures along the Alboran Ridge, supplying valuable information on tsunamis generated by this mechanism in the Alboran Sea, a Western Mediterranean region where information about this source of tsunamis is scarce. For this purpose, we have numerically simulated the triggering of a tsunami by a submarine landslide on the southern flank of the Alboran Ridge. This simulation allows us to analyse the factors controlling tsunami wave propagation and its impact on coastlines of the Alboran Sea.

2. Geological setting

2.1. Tectonics and physiography

The Alboran Sea basin is located in the extensional back-arc domain of the Betic–Rif orogenic belt (Gibraltar Arc), which is the western end of the Mediterranean Alpine Compressive Belt (Fig. 1). These tectonic features have been generated by the westward migration of the Alboran Crustal Domain since the late Oligocene (Platt et al., 2003). This region shows intense deformation as a consequence of the oblique convergence between the Eurasian and African plates from the Late Miocene to Quaternary (Martínez-García et al., 2013). It is characterized by the generation of a broad deformation area and strain partitioning (de Vicente et al., 2008; Vegas et al., 2008). The Alboran Sea basin is an active geological region as indicated by the number of seismic events taking place and its physiographic and tectonic characteristics.

Regional seismicity shows a large number of events of mostly low to moderate magnitudes, under M5 (Buforn et al., 2004). However, some places have high-magnitude earthquakes, such as Adra, in South Iberia (M6.1 in 1910; Stich et al., 2003) or, especially, the Al Hoceima region (Morocco) in the African margin, recently affected by two strong seismic events in only 10 years (M6.0 in 1994 and M6.3 in 2004; Stich et al., 2005). The great variety of focal earthquake mechanisms ranging from pure thrust to strike slip and normal faulting (Stich et al., 2006; Fernández-Ibáñez et al., 2007; de Vicente et al., 2008; Stich et al., 2010) and the presence of penetrative linear structures on the seafloor evidence the intense and varied active tectonics in this region.

The tectonic and physiographic features are represented by the continental margin basement tilting to its interior, which has determined the width (5 to 20 km) of the present-day continental shelves, the presence of two marginal platforms on the slope (Moulouya Marginal Plateau on the Moroccan–Algerian margin and the Djibouti-Motril Marginal Plateau on the South Iberian margin), and seamounts. The most active tectonic feature is a family of NNE–SSW left-lateral strike-slip faults (located between the Al Idrissi Fault (Martínez-García et al., 2013) and NW–SE right-lateral strike-slip faults, such as the Yussuf Fault) that produces ridges, scarps, and depressions on the seafloor (Gràcia et al., 2006; Ballesteros et al., 2008; Vázquez et al., 2008).

2.2. Submarine landslides and controlling factors

Several submarine landslides have been described in this active geological context, (Fig. 1B), both on the slope of the basin margins, such as the Baraza Slide (Casas et al., 2011), and on the flanks of the main seamounts (Martínez-García et al., 2009, 2011; Alonso et al., 2010, 2012, 2014; Vázquez et al., 2010, 2014). These instability processes are largely controlled by tectonic activity, which has been causing continuous seismicity and progressive basin floor deformation since the Late Miocene (Martínez-García et al., 2013).

The continental margins of the Alboran Sea basin have been tilted from the Tortonian to the present by the uplift of the cordilleras around the basin: the Betics Ranges to the north and the Rif Ranges to the south. The Betics Cordillera uplift is marked by the presence of Tortonian carbonate reefs at 1000 m in elevation (Braga et al., 2003) and by current GPS measurements series (Giménez et al., 2000). This uplift produces significant sedimentary transfer from the land masses to the sea. Together with water mass dynamics (Ercilla et al., 2012), this could be responsible for the accumulation of sedimentary units characterized by high sedimentary rates (0.2 mm/a) and the deposition of weak layers with high pore pressure (Casas et al., 2011), which may be liable to generating submarine landslides in the middle or lower slopes, as in the Baraza Slide case.

On the southern flanks of the Alboran Ridge, several chaotic and transparent bodies have been mapped and interpreted as submarine landslide deposits (Vázquez et al., 2013) (Figs. 1B and 2A). The scar zones of mapped submarine landslides are located at water depths of up to 70 m and so are not affected by the action of storm wave loadings. The Alboran Ridge is isolated from continental sediment input sources and therefore has no significant Holocene sedimentary accumulations on its upper slope (Bárcenas, 2002; Bárcenas et al., 2004). In consequence, there are no recent sedimentary overburden processes affecting the upper slope. In addition, major sea-level changes affected the shelf break (around 110–120 m water depth), but they should not have caused notable sedimentary instabilities even during the large-amplitude and high-frequency Late-Quaternary sea-level changes due to the starved character of the upper slope (Bárcenas, 2002; Bárcenas et al., 2004). Likewise, acoustic anomalies related to free gas within sediments or gas hydrates have not been identified in high-resolution seismic profiles (Vázquez et al., 2012, 2014).

Therefore, seismicity and related deformation play a major role in submarine landslide generation in the Alboran region, as evidenced by the numerous seismic events (more than 8000 events in the last 12 years, with more than 1100 of these with a magnitude of over 3.0, IGN earthquake catalogue). In the Alboran Ridge area, 450 earthquakes have been recorded for this period, 22 with a magnitude of over 3.0. Thus, the cumulative effect of seismicity, added to the uplift of the main reliefs, may result in the overcoming of the breaking strength of sedimentary formations on the flanks of the Alboran Ridge and, as a consequence, generate submarine landslides.

2.3. Tsunamis in the Alboran Sea region

A compilation of known historical data on tsunamis in the Mediterranean Sea provides scarce information (Papadopoulos et al., 2014), even more so for the Alboran Sea basin. Tsunamis in the Alboran Sea have occurred with different return periods, with a mean recurrence period of approximately 100 years, and a maximum intensity of 3–5 according to the Sieberg scale (Soloviev et al., 2000). In their book, Soloviev et al. (2000) described a total of 300 events in the Mediterranean Sea, dividing them into different groups according to the intensity of the tsunami-generating process (that is, according to

the period T of wave repetition and the maximum intensity of the tsunami waves, i_{max}). Then, they set up a period T for the Spanish coast, T ≈ 100 years. As the majority of recorded tsunamis on the Spanish Mediterranean affected the Alboran Sea, we assume that this periodicity of 100 years is suitable for the area.

Analysing tsunamis occurring in the twentieth century, for which there are coastal instrumental data records, suggests that maximum amplitudes range between a very modest 15 to 33 cm on the Alboran Sea coasts (Soloviev et al., 1992). These historical low values (compared to neighbouring regions such as the South Balearic Sea or the Algerian Sea) must be explained by the shallower physiography of the Alboran Sea basin with respect to its neighbours and by the increase in distance between the main earthquake and tsunami sources of the Western Mediterranean, primarily located in Northern Algeria eastwards to the 0° meridian. The similarities between the historical and recorded events indicate they were produced by coseismic deformation offshore and submarine landslides in the North African continental slope, related to submarine landslides (Ambraseys, 1981; Yielding et al., 1981; El-Robrini et al., 1985; Campos Romero, 1989; Soloviev et al., 1992, 1997).

An interesting point is the localization of palaeo-tsunamis by geological tools, especially analysing the sedimentary records onshore. There are not many works of this nature on the Alboran region; however, Reicherter and Becker-Heidmann (2009) have collected sedimentary evidence for a palaeo-tsunami along the southern Spanish coast by means of shallow drilling in the lagoon of Cabo de Gata. Radiocarbon dating of these drill cores has linked tsunami deposits to the 1522 Almería earthquake. Submarine landslides on the continental slope of the Almería margin close to the morphological trace on the seafloor of the left-lateral strike-slip Carboneras-La Serrata Fault (García et al., 2006) have been used by Reicherter and Becker-Heidmann (2009) to propose that seismic shaking related to this fault triggered submarine slides in the Gulf of Almería, which ultimately may have caused tsunami waves.

3. Al-Borani canyon and associated deposits

Submarine fans and submarine landslides have been recognized on the southern flanks of the Alboran Ridge (Fig. 2A). Two submarine canyon-fans have been observed in this area, termed the Al-Borani (Fig. 2B) and the Piedra Escuela Canyon-Fans (Bárcenas, 2002; Bárcenas et al., 2004). The Al-Borani system has a buried submarine landslide underlying the fan deposits in seismic reflection profiles (Fig. 3).

The current erosional and depositional morphological features have been recognized in this area (Fig. 2B). Mainly erosional features such as canyons, gullies, and scars have been differentiated on the slope. The Al-Borani canyon extends from the shelf break (110–120 m water depth) downslope to 800 m water depth (lower slope), with an average gradient of 12°. The upper canyon (110–350 m depth) trends WNW–ESE and contains most of the gullies. The lower canyon (350–800 m depth) is oriented NNE–SSW and becomes steeper (up to 19°) around 700 m water depth. Gullies occur from the main canyon up to 150–200 m. Scars are horseshoe-shaped and affect the insular shelf break of the Alboran Island bank, occurring between 70 and 300 m water depth. In the header area, scars have high-angle scarps (average slope of 20° and a maximal slope of 35°) and are 1.5 to 7 km in length. Depositional features are located at the base of the slope-basin floor, where the Al-Borani Fan occurs. This fan is lobate, with a maximum width of 7 km and a length of about 7.7 km, and extends from 800 to 1,100 m water depth with a gentler gradient (1°–4°). It has two main NNW–SSE turbidite channels, small distributary channels, overbank deposits, and lobe deposits (Fig. 3B).

Seismic reflection profiles (Fig. 3) reveal a submarine landslide in front of the canyon mouth, under the current submarine fan. It is characterized by chaotic seismic facies, erosional facies, and a general lenticular geometry. It has an average thickness of 50 ms twtt (up to 80 ms twtt) and an area of at least 50 km^2. Its NW–SE profile (Fig. 3A) shows a wedge extending from the slope towards the basin floor. Its base is clearly erosional both in the proximal area, where its lower boundary continues with the canyon base, and in the distal area. The NE–SW profile (Fig. 3B) also reveals an erosional and highly irregular base and its areal coincidence with recent submarine fan deposits, as well as its similar average thickness. There are several seismic units interpreted as submarine landslides in seismic profiles (Fig. 3), but the Al-Borani landslide is the only one in front of the canyon mouth.

The main erosional scars affecting the shelf and the upper slope of the Al-Borani canyon area could be interpreted in origin as the head of a submarine landslide, but the canyon and gullies correspond to present turbiditic dynamics. It is important to note that the extension of the modern submarine fan coincides with the extension of a buried submarine landslide, as revealed by the high-resolution seismic profiles (Fig. 3). The initial submarine landslide could have been triggered by a major seismic event related to the tectonic activity of the Alboran Ridge structure and nearby active faults such as the NNE–SSW Al Idrissi or WNW–ESE Yussuf faults (Gràcia et al., 2006). In fact, the two segments of the canyon are structurally controlled by faults of these two different fault systems, which have also conditioned the relief of the submarine configuration of Alboran Island (Maestro-González et al., 2008). Seismic reflection surveys allow us to differentiate between modern turbiditic deposits and a previous submarine landslide in the stratigraphic sedimentary record and, therefore, propose relative dating of different sedimentary units (Fig. 3). Seismic stratigraphic techniques, calibrated with ODP wells, tentatively suggest that this submarine landslide could have occurred in the last 0.3 My (Vázquez et al., 2013).

4. Review of tsunami modelling

Tsunami waves have been extensively simulated as long waves whose propagation through deep water can be modelled by shallow-water equations. When interactions with shallow and abrupt topography or flooding effects are to be considered, nonlinear shallow-water systems are commonly used (see references on models below). This long-wave approach is a good approximation for submarine earthquake-generated tsunamis, but it is debatable for landslide-generated tsunamis, at least in the initial generation phase, where enormous localized waves are produced. Despite this, nonlinear shallow-water models have been used for this purpose, producing good results (see, for example, the extreme case of the Lituya Bay Mega-Tsunami for an aerial landslide-generated tsunami in González-Vida et al. (2014)). In addition, an estimate of the ratio between water depth and wavelength in the initial phase of tsunami generation shows low values (around 0.05, for 500 m/10 km), which further justifies use of the kind of models in the scenario considered in this study.

The role of dispersion in the field of tsunami modelling and its numerical simulation is also a key question that arises recurrently in the tsunami wave modelling community. Glimsdal et al. (2013) have addressed this question, pointing out that frequency dispersion is of less importance for earthquake-generated tsunamis and waves generated by large and subcritical submarine landslides, that is, when the Froude numbers of the slide material are not large, as is shown below to occur here. In these cases, dispersive effects are not supposed to be relevant. In any case, it has been shown in Dutykh et al. (2013) that, even if tsunami travelling wave geometry differs when dispersive effects are neglected, shallow-water equations are sufficient to predict maximum run-up values and the inundation area, which in fact is the main objective of risk assessment studies.

Finally, the numerical simulation of earthquake-generated tsunamis and submarine or aerial landslide-generated tsunamis requires quite different modelling approaches if the latter are modelled as completely coupled systems. While earthquake-generated tsunamis have been widely modelled and numerically simulated (e.g., Kowalik and Murty (1993); Satake (1995) for non-linear Shallow-Water hydrostatic models, Grilli et al. (2012) for Boussinesq non-hydrostatic models;

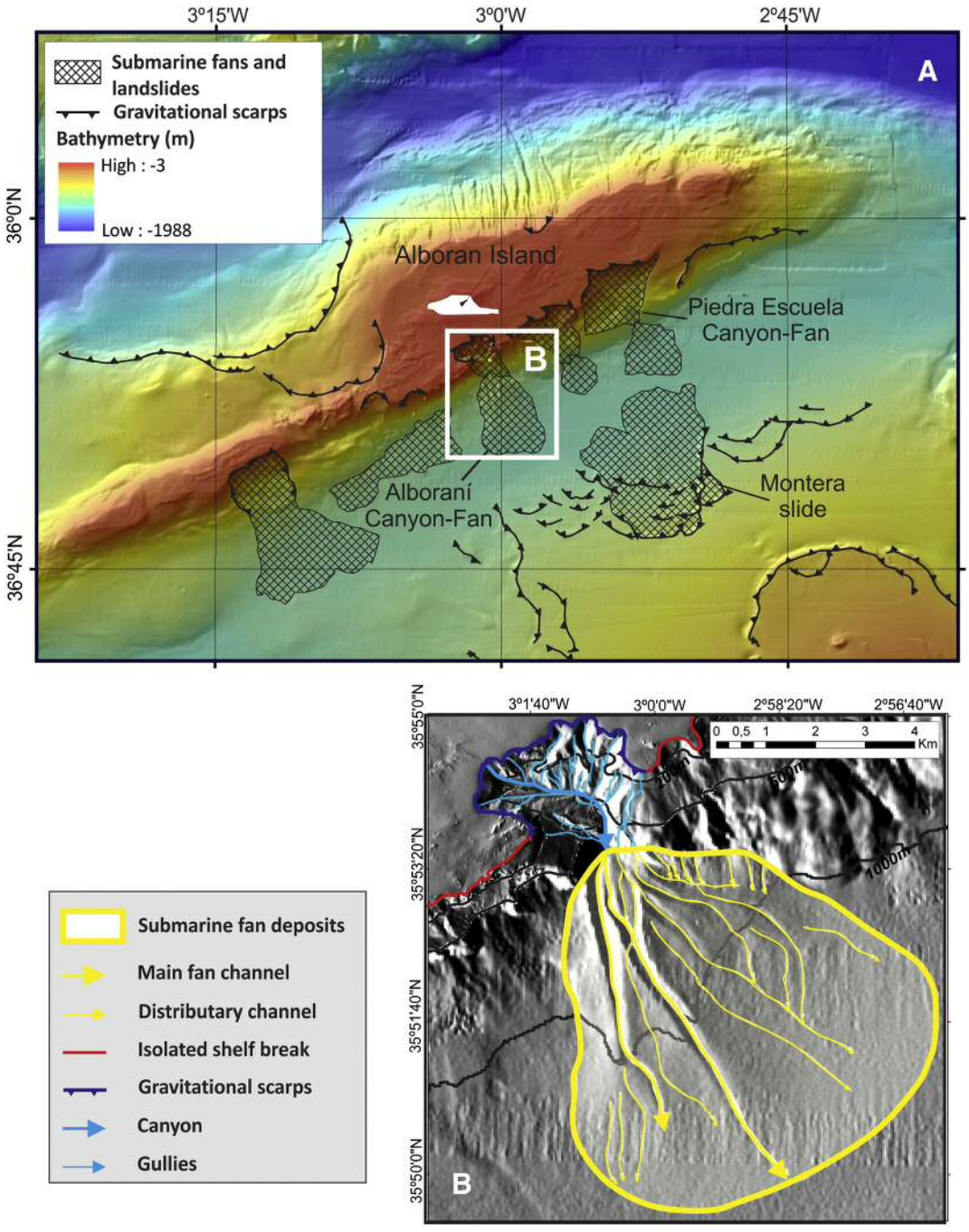

Fig. 2. (A) Digital Terrain Model of the Alboran Ridge northern segment based on a compilation of multibeam bathymetry and location of the main submarine fans and landslides. (B) Morphological features of the Al-Borani Canyon-Fan.

Titov and González (1997); COMCOT model), numerical simulations of coupled dynamic models for landslide-generated tsunamis are still limited (Heinrich et al., 2001; Shigihara et al., 2006). Nevertheless, much work has been done to model these phenomena following other uncoupled approaches, where generation and propagation phases are split (for example in Lastras et al. (2005) and Iglesias et al. (2012), which contains a conceptual model of the Big'95 submarine landslide and numerical simulation of the propagation of the tsunami wave generated; Skvortsov (2002); Watts et al. (2003); Fine et al. (2005); Tinti et al. (2006); Tinti et al. (2011)).

In this work, our modelling and numerical simulation efforts focus on submarine landslide-generated tsunamis based on a fully coupled two-layer system. Unlike Shigihara et al. (2006), who use finite differences techniques, we implement finite volume methods for solving model equations. In Heinrich et al. (2001), a weak coupling on the pressure terms is considered. In these two studies, model equations and parameterizations differ slightly from the ones used here. For example, in Heinrich et al. (2001), pressure and friction terms are different, and in Shigihara et al. (2006) friction is not parameterized by means of a Coulomb term. Moreover, the HySEA landslide-generated tsunami module also implements wet/dry fronts (Castro et al., 2005, 2012; Macías et al., 2013). Therefore, the HySEA code is able to compute the flooded coastal area and run-up heights (when a suitable description of the coast topography is provided) as direct model output (Macías

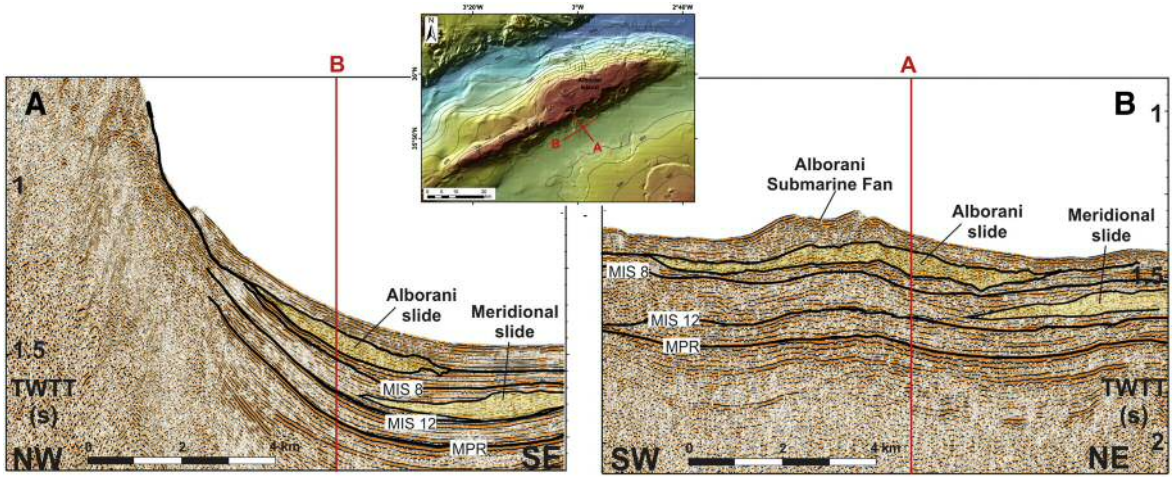

Fig. 3. (A) and (B) High-resolution seismic profiles of the Al-Borani submarine fan and landslides on the South Alboran basin floor. Underlying stratigraphic record of the modern submarine fan. There are several bodies with chaotic seismic facies that are interpreted as submarine landslides; the most recent one is the Al-Borani landslide modelled in this work.

et al., 2015). In addition, the size of the numerical problem treated here is enormous, covering a marine area of 190 × 180 km with a spatial resolution of 25 m, which results in some 55 million computational volumes (compare this, for example, with the 300,000 volumes of Heinrich et al. (2001) for the Papua New Guinea event). In this study, the HySEA landslide–tsunami numerical model (Castro et al., 2005, 2006; Gallardo et al., 2007; Castro et al., 2008, 2012; de la Asunción et al., 2013; Macías et al., 2013) developed by the EDANYA research group (edanya.uma.es) is applied to the hindcasting of the Al-Borani submarine landslide.

5. Methodology

This study is supported by three basic components. First, the hypothesis on which the present study is based; second, the data necessary to recreate the scenario prior to the slide and to support the working hypothesis; and third, the numerical model used to reproduce the hypothesized event.

5.1. Working hypothesis

The basic assumption of this work is the hypothesis that the Al-Borani canyon was initially generated by a massive movement of materials originally located in the upper slope of the southern flank of the Alboran Ridge. This instability process likely also produced the sedimentation of a submarine landslide on the basin floor (forming a submarine lenticular deposit) once all the displaced material had been deposited. This massive slide was probably triggered by a seismotectonic movement. The submarine landslide should have produced a tsunami that affected the coasts of the Alboran Sea. Sedimentary dynamics through the main head scarp of this slide have produced a submarine canyon-deep sea fan system at the same place as the slide (Figs. 2 and 3).

For this study, we have assumed that the landslide took place in one and only one major event. The movement of material caused by the landslide, from its headwaters to its depositional area, would have produced rapid disruption of the seafloor. This disturbance would have been transmitted to the body of the water mass just above the point of formation of the landslide, generating a tsunami across the Alboran Sea basin. All these processes are simulated as a whole below by means of a coupled landslide–tsunami model.

5.2. Bathymetric data

The analysis of the triggering area is based on a bathymetric exploration carried out with a multibeam echosounder, Kongsberg Simrad EM-300, acquired by the Instituto Español de Oceanografía (Spanish Oceanography Institute) in the Alboran-02 and Alboran-03 oceanographic surveys. Multibeam data were processed with Caraibes software and integrated in the ArcGIS software suite. The bathymetric data available for this area have a depth-dependent resolution based on that of the echosounder (10 × 10 m for water depths shallower than 200 m, 20 × 20 m for depths of 200–500 m, and 40 × 40 m for areas deeper than 500 m). The bathymetric grid data allowed us to draw slopes, aspect and sun-illumination maps, and also to perform morphologic analyses and quantitative measurements of the submarine landslide, as shown in the Al-Borani landslide description (Fig. 2).

Based on these data, the geomorphology of the submarine landslides and fans has been interpreted and analysed, establishing the erosion and deposition areas. One of these sedimentary systems has been retained to perform a numerical simulation of the underwater landslide and the associated tsunami that the corresponding sediment collapse would have generated when it was triggered.

To perform the numerical simulation of such an event, a hypothetical palaeo-bathymetry of the geomorphological scenario prior to the slide has been reconstructed (Macías et al., 2012) taking into account the location of the submarine landslide in the seismic reflection profiles (Fig. 3). The bathymetry prior to the submarine landslide is reconstructed based on the determination of the total landslide volume. This volume estimate has considered the extension and geometry of the last landslide observed in the seismic profiles (Fig. 3), but the existing seismic net is not fine enough to provide a detailed cartography of this deposit. The seismic signature, thickness, and location of the buried landslide and its present morphology can be used to infer the spatial distribution and final volume of the buried landslide, considering that the present seafloor features (submarine fan) delineate the geometry of this landslide. To do so, high-resolution bathymetric data are needed. The analysis of the main bathymetric trends allows tracing the probable palaeo-bathymetric map of the study area, suppressing erosional irregularities existing at present, and the comparison between the current bathymetry and this palaeo-bathymetry allows the amount of material displaced to be estimated (Fig. 4).

In order to complete the bathymetric and topographic data in the whole of the Alboran Sea and continental areas, the following datasets have been used: 1) multibeam echosounder EM3000D data acquired

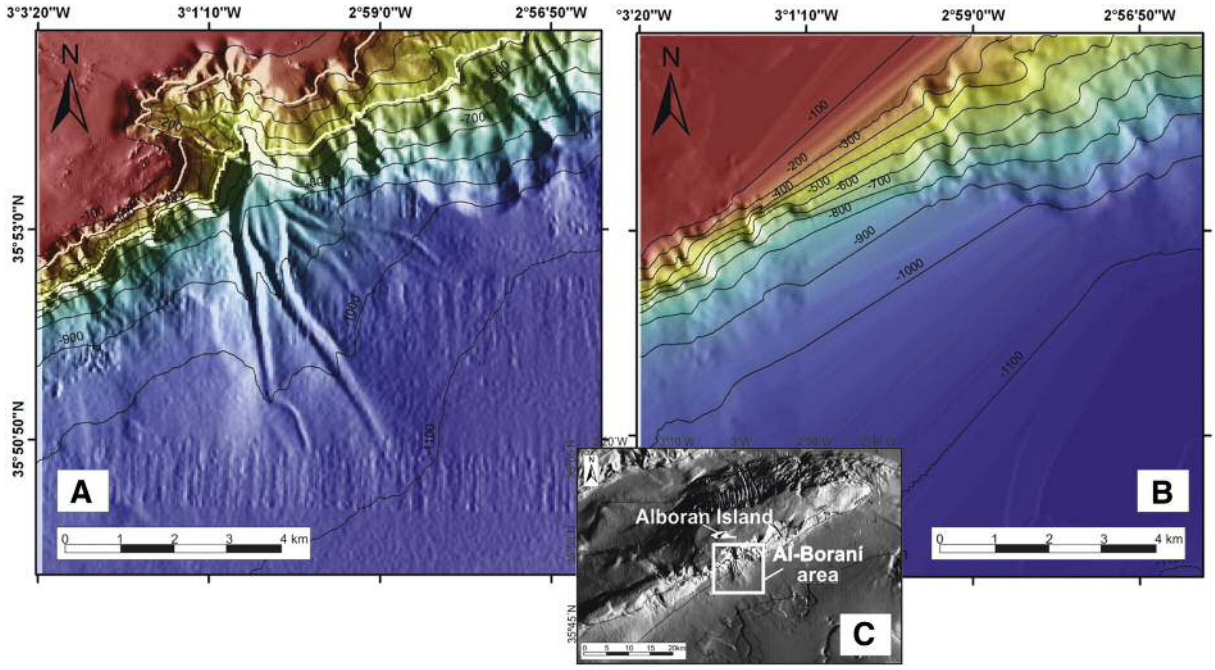

Fig. 4. Al-Borani Canyon area: (A) Actual multibeam bathymetric 3D model of the Al-Borani Canyon-Fan. (B) Hypothetical 3D palaeo-bathymetric model of the previous scenario. (C) Location map.

by the ESPACE project, with a 5 m resolution for the Iberian continental platform; 2) bathymetric and topographic data from the General Bathymetric Chart of the Ocean, with 1.8 km resolution where no other data were available (south 35.65°N); and 3) topographic data from the Digital Terrain Model edited by the Junta de Andalucía, with a 10 × 10 m resolution. The more than 100 million bits of topo-bathymetric data used occupied 3 Gb of memory. From this global file, depths at required mesh points are interpolated.

5.3. Model equations and discretization

The HySEA landslide-tsunami model is used to simulate the submarine landslide, the tsunami generated, its propagation and finally the inundation of the shoreline. This code implements the natural 2D extension of the 1D two-layer Savage–Hutter model presented in Fernández-Nieto et al. (2008) where Cartesian coordinates are used instead of local coordinates at each point of the 2D domain and where no anisotropy effects are taken into account in the normal stress tensor of the solid phase.

The HySEA model has been fully validated using all of NOAA's National Tsunami Mitigation Program (NTHMP) mandatory benchmarks (EDANYA Group, 2015). [See *Notes about HySEA model* in the additional material for further details about the HySEA model].

The mathematical model consists of two systems of equations that are coupled: the model for the slide material is represented by a Savage–Hutter type of model (Savage and Hutter, 1989) and the water dynamics model represented by the shallow water equations (see Fernández-Nieto et al., 2008).

One of the most important features of the model is that both the dynamics of the sedimentary fluidized material and the seawater layer are coupled and each of these two phases influences the other one instantly and they are computed simultaneously. These coupled effects were first studied in a 1D model by Jiang and Leblond (1992), who concluded that these effects are significant for cases of smaller slide material density and shallower waters. Here both conditions are verified as the sediment layer is assumed to be composed of a fluidized debris with $r = \rho_1/\rho_2 = 0.5$, and the initial location of the mass of unstable sediments ranges from 100 to 600 m depth. Nevertheless, the importance of numerically treating in a coupled mode phenomena that are physically coupled have been studied, for example, in Castro et al. (2011a) for the case of two layer shallow water fluids, and in Cordier et al. (2011) for sediment transport models. An uncoupled numerical treatment of these systems may generate spurious oscillations at the water surface or the interface.

The mathematical model implemented in the HySEA landslide–tsunami code consists of a stratified media of two layers (Fig. 5): the first layer is composed of a homogeneous inviscid fluid with constant density ρ_1, (seawater here) and the second layer represents the fluidized granular material with density ρ_s and porosity ψ_0. We assume that the mean density of the fluidized debris is constant and equals to $\rho_2 = (1 - \psi_0)\rho_s + \psi_0\rho_1$ and that the two fluids (water and fluidized debris) are immiscible.

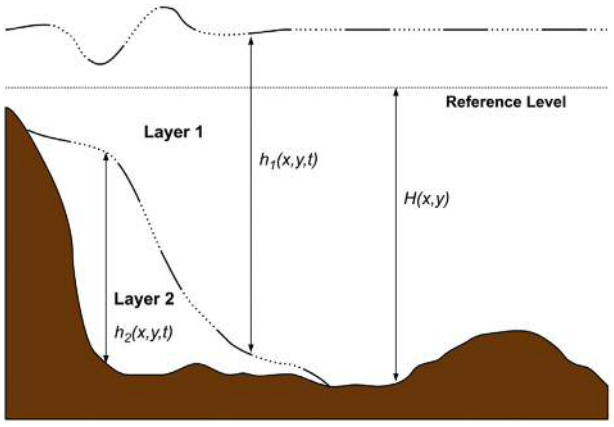

Fig. 5. Sketch of the two-layer Savage–Hutter submarine landslide numerical model. Layer 1 stands for sea water, layer 2 for the fluidized granular material, h_1 and h_2 are corresponding layer thickness, and H is seafloor depth from mean sea level.

The resulting system of equations writes as follows:

$$\begin{aligned}
&\frac{\partial h_1}{\partial t}+\frac{\partial q_{1,x}}{\partial x}+\frac{\partial q_{1,y}}{\partial y}=0\\
&\frac{\partial q_{1,x}}{\partial t}+\frac{\partial}{\partial x}\left(\frac{q_{1,x}^2}{h_1}+\frac{g}{2}h_1^2\right)+\frac{\partial}{\partial y}\left(\frac{q_{1,x}q_{1,y}}{h_1}\right)=-gh_1\frac{\partial h_2}{\partial x}+gh_1\frac{\partial H}{\partial x}+S_{f_1}(W)\\
&\frac{\partial q_{1,y}}{\partial t}+\frac{\partial}{\partial x}\left(\frac{q_{1,x}q_{1,y}}{h_1}\right)+\frac{\partial}{\partial y}\left(\frac{q_{1,y}^2}{h_1}+\frac{g}{2}h_1^2\right)=-gh_1\frac{\partial h_2}{\partial y}+gh_1\frac{\partial H}{\partial y}+S_{f_2}(W)\\
&\frac{\partial h_2}{\partial t}+\frac{\partial q_{2,x}}{\partial x}+\frac{\partial q_{2,y}}{\partial y}=0\\
&\frac{\partial q_{2,x}}{\partial t}+\frac{\partial}{\partial x}\left(\frac{q_{2,x}^2}{h_2}+\frac{g}{2}h_2^2\right)+\frac{\partial}{\partial y}\left(\frac{q_{2,x}q_{2,y}}{h_2}\right)=-grh_2\frac{\partial h_1}{\partial x}+gh_2\frac{\partial H}{\partial x}+S_{f_3}(W)+\tau_x\\
&\frac{\partial q_{2,y}}{\partial t}+\frac{\partial}{\partial x}\left(\frac{q_{2,x}q_{2,y}}{h_2}\right)+\frac{\partial}{\partial y}\left(\frac{q_{2,y}^2}{h_2}+\frac{g}{2}h_2^2\right)=-grh_2\frac{\partial h_1}{\partial y}+gh_2\frac{\partial H}{\partial y}+S_{f_4}(W)+\tau_y
\end{aligned}\tag{1}$$

In these equations, index 1 corresponds to the upper layer and index 2 to the second layer. $h_i(x, y, t)$, $i = 1, 2$ is the layer thickness at each point (x, y) at time t, therefore h_2 stands for the thickness of the slide layer material; $H(x, y)$ is the fixed bathymetry at (x, y) measured from a given reference level, $q_i(x, y, t)$, $i = 1, 2$ is the discharge and is related to the mean velocity by the equation $u_i(x, y, t) = q_i(x, y, t)/h_i(x, y, t)$, g is the gravitational acceleration and r is the ratio of densities $r = \rho_1/\rho_2$.

Terms $S_{f_i}(W), i = 1, \ldots, 4$ model the different effects of the dynamical friction while $\tau = (\tau_x, \tau_y)$ corresponds to the static Coulomb friction term. The terms S_{f_i} are defined as follows:

$$\begin{aligned}
&S_{f_1}(W)=S_{c_x}(W)+S_{a_x}(W), \qquad S_{f_2}(W)=S_{c_y}(W)+S_{a_y}(W),\\
&S_{f_3}(W)=-rS_{c_x}(W)+S_{b_x}(W), \quad S_{f_4}(W)=-rS_{c_y}(W)+S_{b_y}(W),
\end{aligned}$$

where $S_c(W)=\left(S_{c_x}(W), S_{c_y}(W)\right)$ parametrizes the friction between layers and it is defined as follows:

$$\begin{cases}
S_{c_x}(W)=m_f\dfrac{h_1h_2}{h_2+rh_1}\left(u_{2,x}-u_{1,x}\right)\|u_2-u_1\|\\
S_{c_y}(W)=m_f\dfrac{h_1h_2}{h_2+rh_1}\left(u_{2,y}-u_{1,y}\right)\|u_2-u_1\|
\end{cases}$$

being m_f a positive constant.

$S_a(W)=\left(S_{a_x}(W), S_{a_y}(W)\right)$ parametrizes the friction between the water and the fixed bottom topography, if there is no granular material and it is defined by a Manning friction law:

$$\begin{cases}
S_{a_x}(W)=-gh_1\dfrac{n_1^2}{h_1^{4/3}}u_{1,x}\|u_1\|\\
S_{a_y}(W)=-gh_1\dfrac{n_1^2}{h_1^{4/3}}u_{1,y}\|u_1\|
\end{cases}$$

where $n_1 > 0$ is the Manning coefficient, between the water and the fixed bottom topography.

$S_b(W)=\left(S_{b_x}(W), S_{b_y}(W)\right)$ parametrizes the dynamical friction between the debris layer and the fixed bottom topography and, as in the previous case, it is defined using a Manning law:

$$\begin{cases}
S_{b_x}(W)=-gh_2\dfrac{n_2^2}{h_2^{4/3}}u_{2,x}\|u_2\|\\
S_{b_y}(W)=-gh_2\dfrac{n_2^2}{h_2^{4/3}}u_{2,y}\|u_2\|
\end{cases}$$

where $n_2 > 0$ is the corresponding Manning coefficient.

Finally, $\tau = (\tau_x, \tau_y)$ is the static Coulomb friction term and it is defined by

$$\begin{aligned}
&\text{if } \|\tau\|\geq\sigma^c\Rightarrow\begin{cases}\tau_x=-g(1-r)h_2\dfrac{q_{2,x}}{\|q_2\|}\tan(\alpha)\\ \tau_y=-g(1-r)h_2\dfrac{q_{2,y}}{\|q_2\|}\tan(\alpha)\end{cases}\\
&\text{if } \|\tau\|<\sigma^c\Rightarrow q_{2,x}=0,\quad q_{2,y}=0,
\end{aligned}$$

where $\sigma^c = g(1 - r)h_2 \tan(\alpha)$, being α the Coulomb friction angle. The above expression models the fact that a critical slope is needed to trigger the slide movement. It must be taken into account that the effects of hydroplaning may be important for submarine mass failures and tsunami generation (Harbitz et al., 2003).

The discretization of system 1 is performed by an explicit first order IFCP Finite Volume Scheme where the discretization of the Coulomb friction term is performed following Fernández-Nieto et al. (2008) (see Fernández-Nieto et al. (2011) for details on the stability, convergence and efficiency of the numerical scheme). The resulting scheme has been implemented in Graphics Processors Units (GPUs) using CUDA, achieving a speed-up of two-order of magnitude compared to a conventional CPU implementation (see Castro et al. (2011b) for a review and de la Asunción et al. (2012)). This methodology allows us to considerably improve the efficiency of the algorithm as well as the size of the discrete problems that can be solved.

This model reduces to the usual nonlinear shallow-water (SW) system when the layer of granular material is not present or when it has zero velocity and this layer reaches equilibrium. Therefore, the model can be used to numerically reproduce the different stages of a landslide tsunami simulation: the landslide tsunami generation, the farfield wave propagation and, finally, the coastline inundation and the run-up height reached by the tsunami wave.

6. The numerical simulation

The Al-Borani erosional and depositional features were used to assess the impact of a tsunami generated by one submarine landslide since it has a well-defined morphology, with an upper area characterized by major horseshoe scars at the shelf break and upper slope, eroded by a segment canyon, and a lower area characterized by a set of depositional units at the mouth of the canyon on the bottom of the SAB comprising a submarine fan and a prior submarine landslide (Figs. 2B and 3).

The initial stage for the numerical simulation consists of a linear upper slope, without erosional scars (Fig. 4B). The numerical simulation starts with the rupture of this slope and the shift to the bottom of the SAB of a mass of materials equivalent to the current submarine deposit. The initial bottom morphology prior to the slide in the Al-Borani area is reconstructed in two steps. The first one consists in filling the current canyon and scar area with sedimentary materials. In order to preserve the mass volume, the amount of material needed to do so is estimated, and the same volume of material is removed from the submarine deposit onto the SAB to recover an approximation of the seafloor prior to the event. Thus, the present sedimentary deposit should be approximately reconstructed once the simulated slide takes place.

The numerical grid model is a rectangular mesh of a very high resolution of 25×25 m. The computational domain dimensions are 180 km in length and 190 km in width, which gives 54,720,000 computational cells and some 330 million equations and unknowns to be solved at each time step. In open sea limits, non-reflective boundary conditions are considered and no specific boundary condition is required for the coasts as a numerical treatment of the wet/dry fronts is used (Castro et al., 2005).

6.1. Modelling the submarine landslide

The parameters required by the mathematical model have been set so that the simulated submarine deposit, once the landslide concludes, is as close as possible to the current bathymetry. This aims to reproduce the Al-Borani landslide as reliably as possible. A suitable choice of model parameters is a key factor in the amount of sliding sediment and in the extension of the sedimentary lobe generated on the floor of the canyon. Therefore, model parameter adjustment and data validation with the real bathymetry are essential for a realistic tsunami simulation. Different morphological features can be observed if the simulated bathymetry is compared to the recent seafloor bathymetry (Fig. 6).

The simulated bathymetry is more symmetrical (Fig. 6A), whereas the current sedimentary deposits shifted slightly westwards (Fig. 6B), probably due to the long-term action of the Western Mediterranean Deep Water, which flows south-westwards along the SAB (Hernández-Molina et al., 2011). In addition, the two scours or channels that go through the current submarine fan, from the northwest end to the southeast end, are not reproduced. The scours are generated by the erosion and deposition of sediments that flow downslope and have subsequently been superimposed on the slide. Both morphological differences have been produced by processes with time scales much larger than the tsunami event and model timescales; therefore, they cannot be represented by the simulation nor are they needed for our purposes.

The numerical simulation reproduces a landslide that generates a sedimentary deposit similar in size, shape, and front location to the current submarine fan. Therefore, if the proposed hypothesis of a submarine landslide had in fact taken place, we would expect it to reproduce the associated tsunami and its impacts as happened in the past. [Video 1 (lower panel) shows the animation of the submarine landslide evolution as represented by the numerical model. The most intense phase of the slide occurs during the first two minutes of simulation although the slide material continues moving for much longer.]

Regarding the nature of the simulated submarine landslide, we have computed the two-dimensional map of time varying the slide Froude number, defined as the ratio. $u_2/\sqrt{g h_2}$ [A movie showing the evolution of this variable during the first 10 min of simulation can be found in the additional material (Video 2).] Obviously, the larger values for this Froude number appear in the first stages of the simulation (first 90 s), reaching a maximal local Froude number of 0.6 at t = 50 s (Fig. 7). Despite this value, most of the slide remains at much lower values, below 0.3. Fig. 7 depicts the time evolution of the maximal slide Froude number, computed for values of h_2 larger than a threshold value of hf. When the movement is intense, the computed Froude number is very sensitive to the threshold slide layer depth considered, as shown in Fig. 7. Nevertheless, the computed Froude number is only relevant for sediment layer depths large enough to represent a real displacement of material and not for thin layers of moving sediment (for values of $h_2 > 6$, $Fr_2 < 0.35$). Fig. 8-A shows the spatial distribution of the Froude number at time t = 50 s, when the maximal local value is reached. For large values of h_2 (Fig. 8-B), the slide layer Froude number remains below 0.3. Larger values are only found in the slide boundary region. Therefore, the Froude number computation shows the clear subcritical nature of this submarine landslide, corroborating that frequency dispersion plays a minor role in this event.

6.2. Tsunami wave generation

When the submarine landslide is triggered, the initial wave that it produces is formed by the combination of a positive and a negative perturbation (Figs. 5 and 9-A and B). On the erosion domain of the Al-Borani area, on the upper slope on the southern flank of the Alboran Ridge (Fig. 2), a depression wave has formed, as a consequence of the instantaneous displacement (downward) of the water mass that tends to occupy the space vacated by the sedimentary material moving downslope in the slide. In the depositional domain, currently occupied by the submarine fan, a positive wave is generated by pressure effects related to the fast accumulation of a high kinetic energy sedimentary body at the base of the slope and the adjacent basin floor plane of the SAB.

In the first stages of the simulation (<2 min, Fig. 9), the positive–negative initial wave pattern is maintained. The maximum amplitude of the depression wave (denoted by Dep hereafter) in the submarine landslide generation area reaches −19.62 m, whereas the maximum amplitude above the mean sea level (denoted by Emax) reaches 5.16 m. In these early stages waves propagate elliptically, elongated

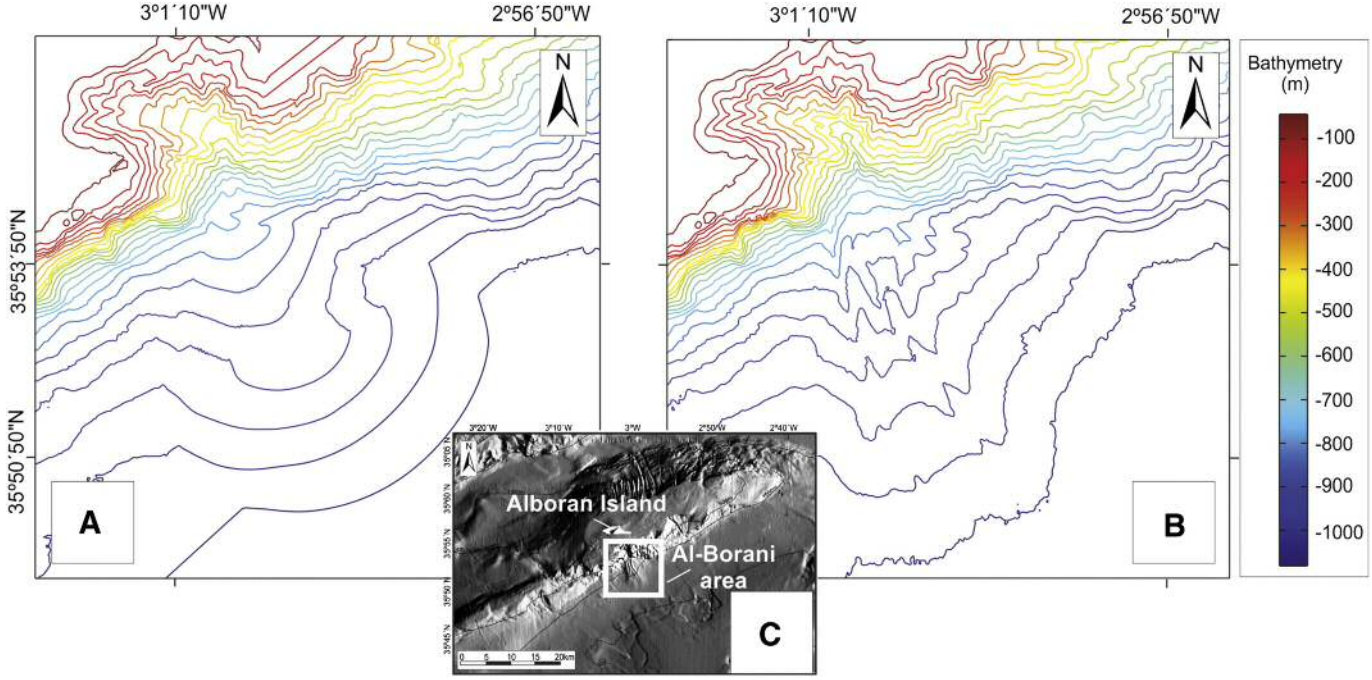

Fig. 6. (A) Bathymetry given by the model after the avalanche. (B) Actual submarine fan bathymetry. (C) Location on the Southern flank of the Alboran Ridge.

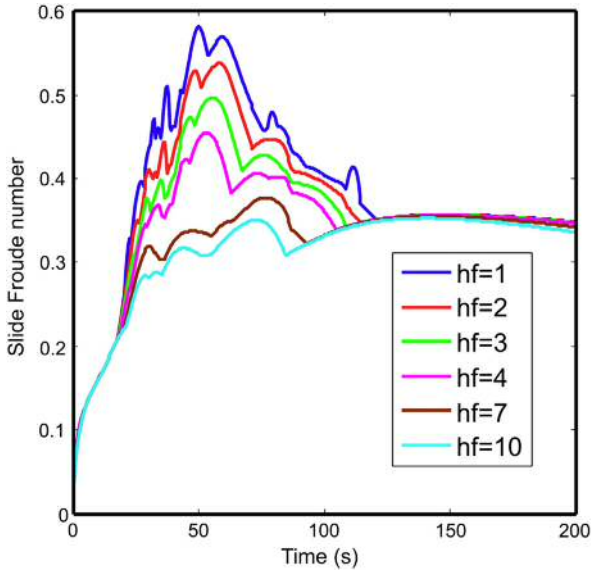

Fig. 7. Time series evolution of the maximal value for the slide Froude number throughout the numerical simulation. hf is the threshold value of the sediment layer thickness, h_2, for computing this Froude number.

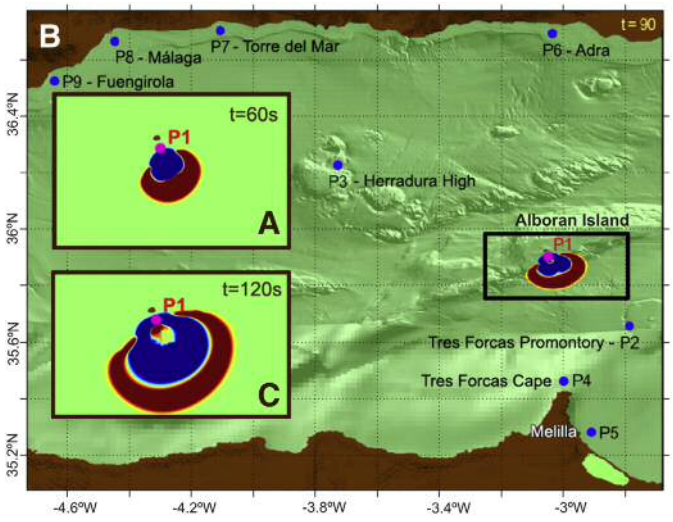

Fig. 9. Initial stages of the numerical simulation. (A) t = 60 s, (B) t = 90 s in the complete domain, and (C) t = 120 s. In red is the positive wave (elevation above mean sea level), in blue is the negative wave (depression). (For interpretation of the references to colour in this figure legend, the reader is referred to the web version of this article.)

NE–SW (Fig. 9). Some asymmetry is produced in relation to the tsunamigenic mechanism and basin relief near the generation area.

An estimate of the ratio between water depth and wavelength at this initial phase of tsunami generation shows small values for this ratio, around ≈0.05, corresponding to 500 m/10 km, which supports the long wave approach.

6.3. Tsunami wave propagation

[The description presented in this section can be followed while watching Video 3 in the Additional Material.] The initial wave starts propagating as a negative disturbance northwards and positive southwards. Propagation velocities are also heterogeneous: waves travelling to the S-SE move faster, towards the low relief of the SAB, whereas waves heading N move slower as they encounter the Alboran Ridge high, which slow down their propagation velocity.

Three minutes after triggering, tsunami waves arrive at control point P1 (near Alboran Island) still exhibiting basically the initial wave characteristics (Fig. 10-A). These heterogeneities cause the wave propagation pattern to present different configurations to the N and to the S. The presence of the Alboran Ridge produces a slowdown of tsunami waves moving northwards and causes clear asymmetry in their propagation (Fig. 11-A).

The higher velocity of waves travelling southwards, conditioned by the relatively open physiography of the SAB, produces a quick tsunami arrival to the North Africa coast, with the wave train coming in 10 min after tsunami generation at Tres Forcas Cape (Emax = 1.7 m, Dep = −1.1 m) (control point P4 in Fig. 11-B). The presence of this cape together with its continuity in a NE–SW oriented underwater promontory, favours the arrival of waves westwards, to the Al Hoceima region, and slows them eastwards. In this way, the local physiography

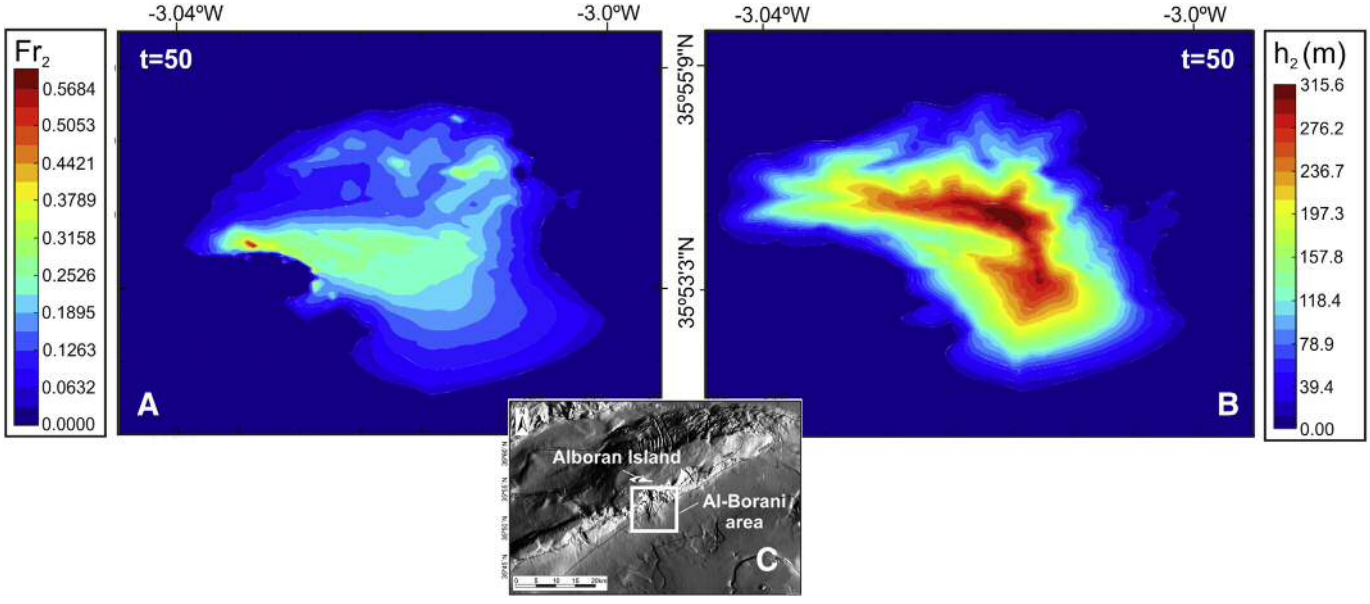

Fig. 8. (A) Snapshot of the slide Froude number spatial distribution at time t = 50 s (when the maximal value is reached). (B) Slide layer thickness (in metres) at t = 50 s. (C) Location of the snapshots.

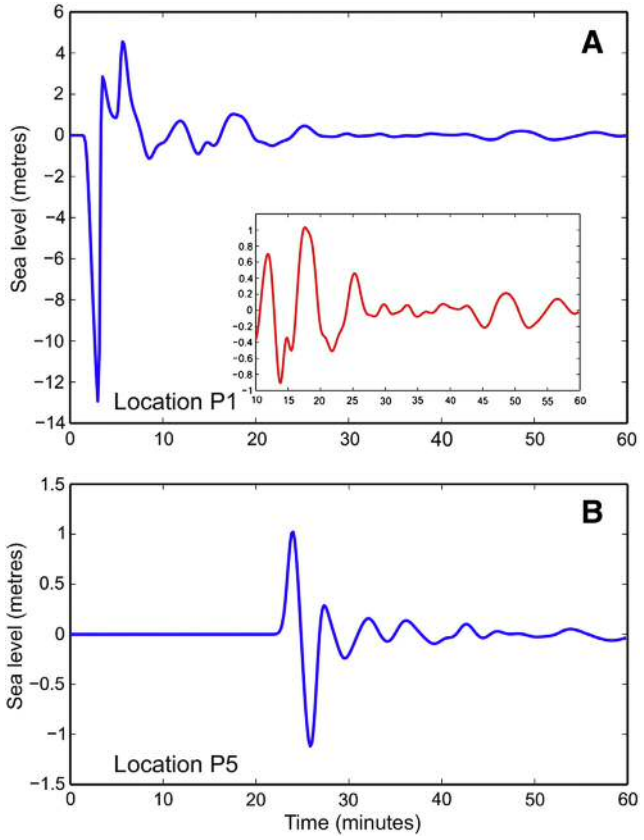

Fig. 10. Sea surface elevation time series at: (A) location P1 (in red a zoom from t = 10 min.) and (B) location P5. (For interpretation of the references to colour in this figure legend, the reader is referred to the web version of this article.)

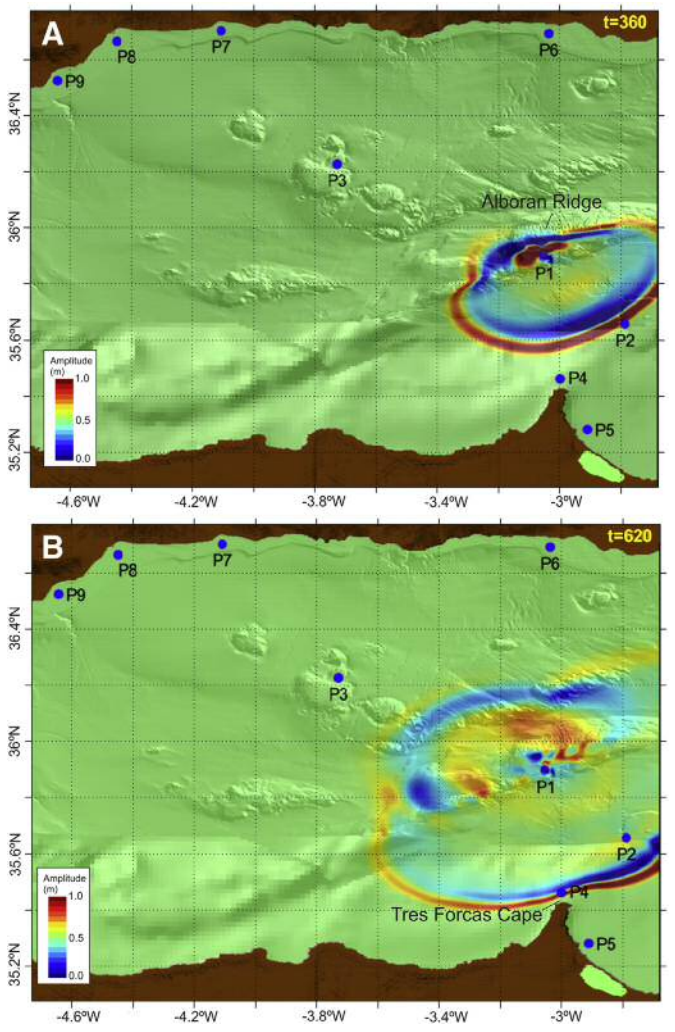

Fig. 11. Time evolution of the generated tsunami wave after: (A) 6 min and (B) 10 min and 20 s. See Fig. 9 for descriptive names for the control points.

partly protects the city of Melilla where waves arrive 22 min after the tsunami triggering (Emax = 1.23 m, Dep = −1.2 m) (control point P6 in Figs. 12-A and 10-B).

To the north tsunami wave propagation is delayed by the Alboran Ridge. The first point on the South Iberian coast that receives the tsunami waves is Sacratif Cape, 22 min after tsunami generation, like Melilla. Sacratif Cape is located in the coast between Motril and Adra, the tsunami wave arriving at this latter city 2 min later (Emax = 0.82 m, Dep = −1.2 m) (control point P6 in Figs. 12-A and 13-A). At this stage, a second main physiographic effect can be observed on the general propagation pattern. Tsunami waves show two different fronts controlled by the smooth slope that constitutes the boundary between the Djibouti-Motril marginal platform and the West Alboran Basin (WAB). The faster wave front travels westwards favoured by the lower relief of the WAB. On the other hand, the second wave front travels northwest and its spread is controlled by the stepped relief of the continental slope in this sector, especially by a series of seamounts aligned between Alboran Island and the city of Málaga (Banks of Djibouti), which slows down this wave in the simulation.

The Banks of Djibouti has a remarkable control effect, with tsunami waves arriving sooner to the city of Fuengirola (t = 34 min, control point P9 in Fig. 12-B) but with a maximum elevation of only approximately 0.1 m for the first impact wave, than to the city of Málaga (35 min, control point P8 in Fig. 12-B) nearer to the tsunami generation point. Finally, in this part of the coast (between Fuengirola and Málaga) significant resonance effects of tsunami waves that interact and amplify are observed (Fig. 12-C, see Video 4 in additional material to appreciate the resonant effects). The maximum elevation corresponds, in Fuengirola, to the third positive arrival wave, as observed at checkpoint P9 (Fig. 13-C) off the coast of this city (t = 43 min, Emax = 0.58 m, Dep = −0.34 m), whereas the highest elevation in the Bay of Málaga also corresponds to the third positive wave (checkpoint P8, Fig. 13-B) 48 min after the tsunami generation (Emax = 0.43 m, Dep = −0.41 m).

The origin of the heterogeneity observed in the simulation can be explained comparing the maximum amplitudes map obtained with the model (Fig. 14) with the arrival time map (Fig. 15) and the bathymetric chart of the Alboran Sea basin floor.

The Alboran Ridge exerts a barrier effect that is reflected in the maximum amplitudes distribution, with the submarine slide generation zone exhibiting the maximum amplitudes, a region of highly elevated amplitude values can also be observed spreading to the south and southeast along the Alboran Ridge, however amplitudes decrease drastically northwards of this ridge and gradually to the west. A notable point has been observed in the maximum amplitude map: all of the main high reliefs of the basin floor produce an amplification of tsunami waves and generate amplitude nucleation over the highest seamounts (Fig. 14). Furthermore, a velocity slowdown has also been noted over the main high relief that produces the alteration in the concentric pattern in the arrival time map (Fig. 15). The distribution of the arrival times appears marked by inflection lines in the propagation pattern. In this regard, the presence of successive seamounts in the northern margin of the Alboran Sea basin produces an amplification of the amplitude however, these seamounts are also responsible for a wave deceleration, and therefore produce a delayed arrival to the coastline near the city of Málaga.

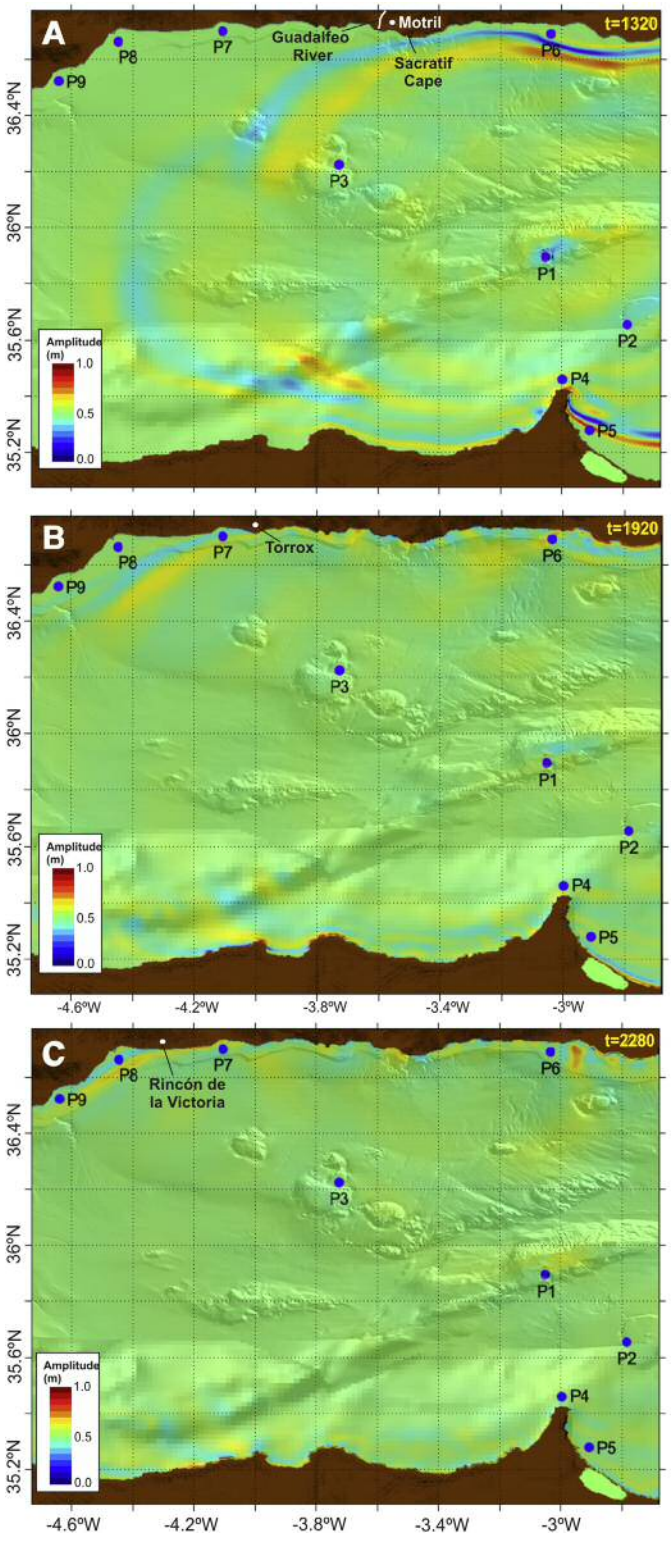

Fig. 12. Tsunami wave arrival on the Southern Iberian coast at different locations. (A) Arrival at the eastern coast (Adra-P6), t = 22 min. (B) Arrival at Torre del Mar (P7), t = 32 min. (C) Arrival at Málaga and its bay (P8), t = 38 min. See Fig. 9 for descriptive names for the control points.

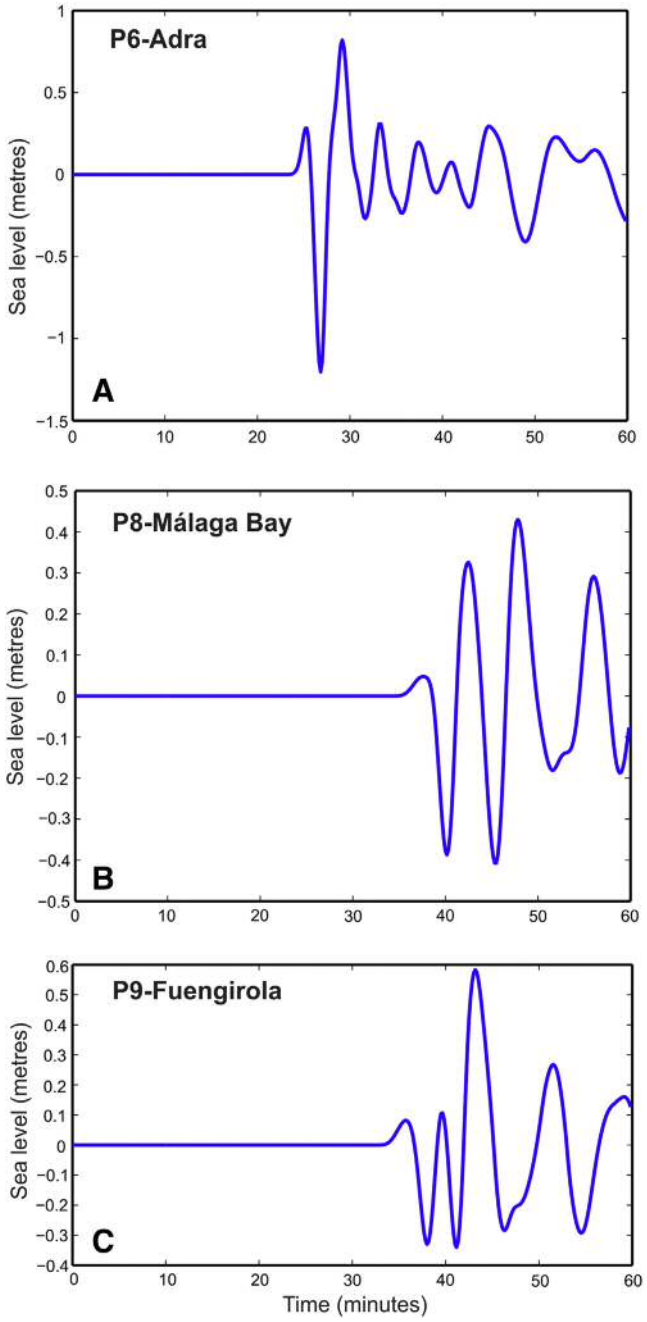

Fig. 13. Sea surface elevation time series at locations: (A) Adra (P6); (B) Málaga Bay (P8), and (C) Fuengirola (P9).

6.4. Impact on the coast

Due to the high resolution of the numerical model, when topographic and bathymetric data are also good enough, some conclusions can be extracted about coastal penetration of the tsunami wave. Therefore, flooding areas are much better resolved along Iberian coasts than on the African shoreline. Model resolution is a quadrangular grid of 25 × 25 m. Topographic data on the Spanish coast have a resolution of 10 m (finer than the computational mesh), whereas in the African coast data are scarce with a resolution of approximately 1.8 km.

The physiographic configuration of the area where the submarine landslide occurred conditioned the general morphology of the waves as follows (see Macías et al. (2012) for further details):

1. when travelling southwards to the African coast, they have a large positive leading crest and depression followed by smaller amplitude disturbances, as can be seen in Fig. 10 for location P5.
2. when travelling northwards towards the Iberian coast, the Alboran Ridge produces a barrier effect, the leading positive elevation is

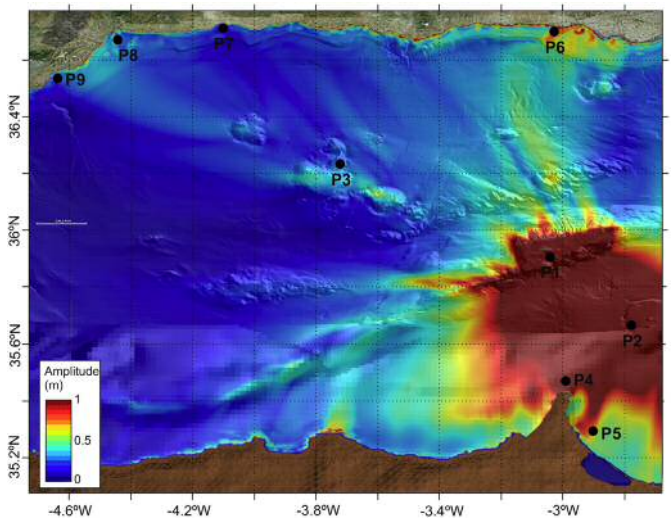

Fig. 14. Maximal height reached by the tsunami wave at each point of the computational domain (highest values in red). See Fig. 9 for descriptive names for the control points. (For interpretation of the references to colour in this figure legend, the reader is referred to the web version of this article.)

small, with the larger perturbation being the second or third peaks, as can be observed in Fig. 13 for locations P6, P8 and P9.

Fig. 16 shows the coastal strip flooded 49 min after the submarine landslide is triggered in the surroundings of the Guadalhorce River mouth, between Málaga and Torremolinos. The size and shape of this strip change over time, increasing when positive waves get to the coast and drying when depression waves get there [see Video 4 to appreciate this behaviour]. One effect that has proven to be important in determining the extent of the flooded area is the arrival of subsequent tsunami waves once the coastal strip has already been flooded. Second and later positive waves, as they flow over already wetted areas, can have a stronger impact even though they are of smaller amplitude due to reduced friction. This is an aspect (considering a reduced friction when water flows over already wetted areas) that has not been taken into account in the present numerical model, meaning that maximal flooding areas may be underestimated. In the next version of the HySEA model, a parameterization of these effects, identifying already inundated areas and imposing a reduced friction coefficient there, will be implemented.

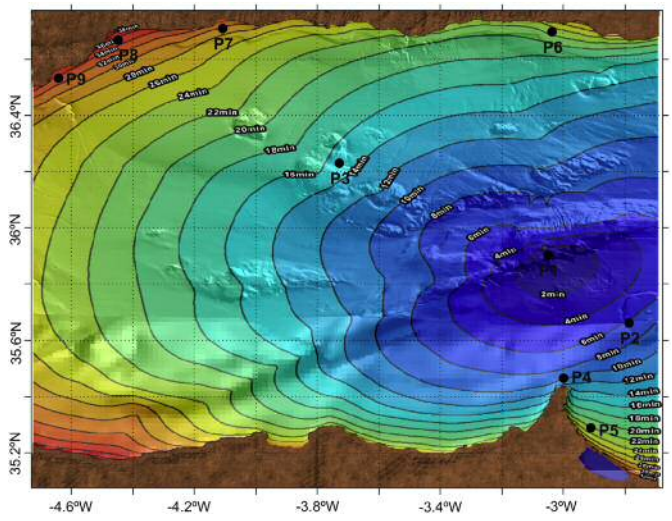

Fig. 15. Isolines showing the arrival times of the leading tsunami wave. See Fig. 9 for descriptive names for the control points.

Summarizing the main flooding effects of the tsunami waves, the following coastal areas have been distinguished:

1. Alboran Island is completely flooded and disappears under the first large tsunami wave that arrives 4 min after generation, when island inundation begins [Video 1, upper panel].
2. Cape Tres Forcas-Melilla area (close to model checkpoints P4 and P5). The abrupt topography of the cape results in limited coastal flooding here, except in local small creeks. In Melilla, the flooded area reaches 350 m. The wave arrives at the island barrier of the Nador Lagoon, east of the city of Melilla, approximately 30 min after generation. The barrier is progressively flooded and 10 min later it has nearly disappeared.
3. The Iberian coast between Campo de Dalias (SW of Almería) and Adra. This is the area most exposed to the tsunami on the Iberian coast. Campo de Dalias is particularly affected by flooding, with up to 900 m inland penetration (Fig. 17). In Adra, where some resonant effects occur, with flooding up to 400 m. [See Video 3 from minutes 28 to 31 for observing resonant effects close to Adra and around minute 34 in the bay to the east].
4. The Iberian coast between Adra and the Gualdalfeo River mouth. Minimal penetration on the Adra-Motril coastal strip and only some noteworthy flooding in creeks of up to 200 m. In the short coastal strip between Motril and the Guadalfeo River mouth, more extensive flooding is observed, with the port of Motril and surroundings being the area of maximal flooding (250 m).
5. The Iberian coast from Torrox to Fuengirola. From east to west, there are several areas of substantial flooding: a large strip from the Torrox River mouth (180 m) to El Rincón de la Victoria (200 m). Near Málaga, several coastal districts are flooded: 150–350 m in eastern Málaga and 350 m in western Málaga. In the mouth of the Guadalhorce River, flooding is more intense, reaching 400 m. The coastal strip between Torremolinos and Fuengirola has flooded areas from 200 to 300 m inland.

7. Discussion

The numerical simulation of a submarine landslide-generated tsunami in the Alboran Sea basin aids in extracting key conclusions regarding wave propagation and risk analysis on coastlines and coastal populations. In the case under study, the simulated submarine landslide produces a deep incision in the reconstructed scenario, which reproduces the palaeo-bathymetry of the Alboran Ridge, resulting later in the formation of the Al-Borani Canyon. The present submarine fan configuration has served to calibrate some model parameters given its thickness and morphological similarities with the previous submarine landslide.

The occurrence of a submarine landslide on the SAB has been estimated at 0.225 My by seismic stratigraphic techniques calibrated with ODP wells for the PlioceneÐQuaternary cover (Vázquez et al., 2013). Nevertheless, this time estimate cannot be taken as the return period for landslide-generated tsunamis all over the Alboran Sea basin as there could exist several other potential landslide sources that could decrease this return period. As well, it is necessary to point out the occurrence of submarine landslides on smooth slopes that do not produce significant changes on the seabed and could have been generated more gradually. This could have happened, for example, with the Montera Slide (Fig. 2B) (Vázquez et al., 2014), which occurred as a sedimentary instability on the surface of a sedimentary deposit on the southern flank of the SAB. Nevertheless, a significant slide deposit is generated on the basin floor, included in the sedimentary record. A future work should catalogue these different sources of ancient landslides by location and then pinpoint areas of potential slide risk. This work, and in particular the HySEA landslide model, together with further onshore field studies, may serve to simulate, analyse, and

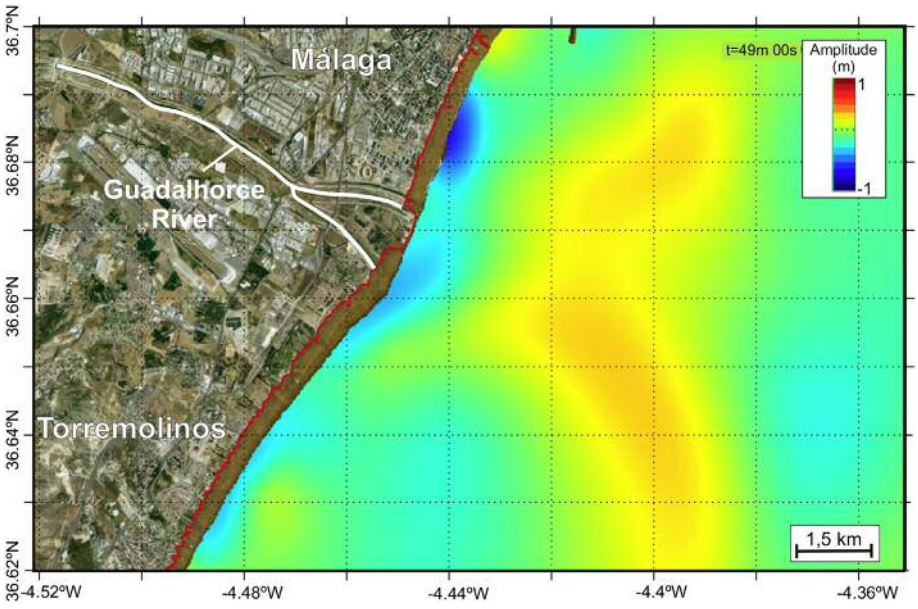

Fig. 16. Simulated flooding at time t = 49 min of the coast line to the west of the city of Málaga, in the surroundings of the Guadalhorce River mouth.

provide us with broader knowledge on the occurrence of events such as the one modelled and simulated herein.

Additionally, we seek to develop and implement a tool that may serve to simulate similar submarine landslides and evaluate their potential flooding risk in coastal areas. This is not a simple task as it requires an initial identification of potential slide areas, and then (and this is the critical part) we must be able to define the slide volume. This may be easy a posteriori, as in the hindcasting example presented here, but harder for forecasting a real case. Large errors in the predicted slide volume would lead to large errors in the numerical predictions.

This study has analysed the geological features of the Alboran Sea basin and the implementation of a coupled very high-resolution numerical model that leads to some important conclusions. Although the numerical simulation shown here corresponds to a unique possible event in one of the submarine landslide sources of the Alboran Sea, the numerical results obtained allow us to infer the approximate impact of tsunami waves generated by a landslide in the central region of the Alboran Sea basin on the different sectors around its coastline. It must be kept in mind that wave amplitude and directionality are conditioned by landslide source and exact location. In this regard, the numerical simulation presented here reveals the existence of three distinct risk areas:

1. Cape Tres Forcas and its surroundings, with the higher risk due to its proximity to the tsunamigenic focus. Furthermore, no submarine obstacle hinders wave propagation.
2. Coast of Adra, with a medium risk due to the slope of the continental shelf, which locally increases wave amplitude.
3. Bay of Málaga, with a lower flooding risk due to the submarine elevations that tsunami waves find on their way to this location and also due to the greater distance to the tsunamigenic source. Nevertheless, the shape of the coast may generate resonant effects [see Video 4 in additional material from minutes 42 to 45 of simulation].

The total volume displaced is around 1000 million m^3 on a maximum slope of 1000 m, which determines the size of the generated initial wave, as well as its impact and penetration in the litoral zone. The magnitude of the initial wave at the generation point is significant, reaching about 14 m elevation and up to about 25 m of depression.

The arrival times are always short, ranging from 12 min to the nearest area, Cape Three Forcas in the African coast, and from 22 to 38 min on the South-Iberian shoreline.

Despite the large initial amplitude of the generated wave, disturbances that come ashore are of much more modest amplitude, with only those areas along the African coast closest to the generation point exhibiting waves of significant amplitude (over 1.7 m). For South-Iberian coasts, arrival amplitude never exceeds one metre, and in the more remote areas (such as Fuengirola) it is below half a metre. In any case, the tsunami that the numerical simulation reproduces is in agreement with the range of amplitudes and shares similar characteristics with those events for which we have a historical record.

Depending on the location of the coastal zone (south or north of the generation area) waveform morphology is different. The initial shape of the wave and the presence of the Alboran Ridge are both key factors in determining this differentiated morphology.

Flooding of the coastal strip is strongly influenced not only by the amplitude of the arrival wave, but also by coastline topography, mainly when it can generate resonant effects.

The numerical simulation of the Al-Borani landslide and associated tsunami allows us to determine the initial characteristics of the tsunami waves generated, to observe and analyse how wave trains propagate, to determine the influence of physiographic features on wave propagation geometry and on the modulation of wave amplitude, and to evaluate the characteristics of the likely tsunami that would have been generated on the coasts of the Alboran Sea.

8. Conclusions

A submarine landslide has been identified by the interpretation of multibeam bathymetry data and high- to very high-resolution seismic profiles. Current seafloor features correspond to a submarine fan, but the erosional scar on the slope could have been generated at an initial stage by a submarine landslide. Landslide deposits are located under the submarine fan and show a similar size, so the submarine fan's location likely replicates the previous landslide deposits. The mathematical modelling and numerical hindcast simulation of a hypothesized ancient submarine landslide in the Alboran Sea basin and the associated tsunami have been performed. The possible tsunami originated by this submarine landslide has been numerically simulated. This submarine landslide, located in front of the Al-Borani canyon mouth on the southern Alboran Ridge slope, is currently part of a turbidite system, forming a submarine canyon-sedimentary fan system known as the Al-Borani

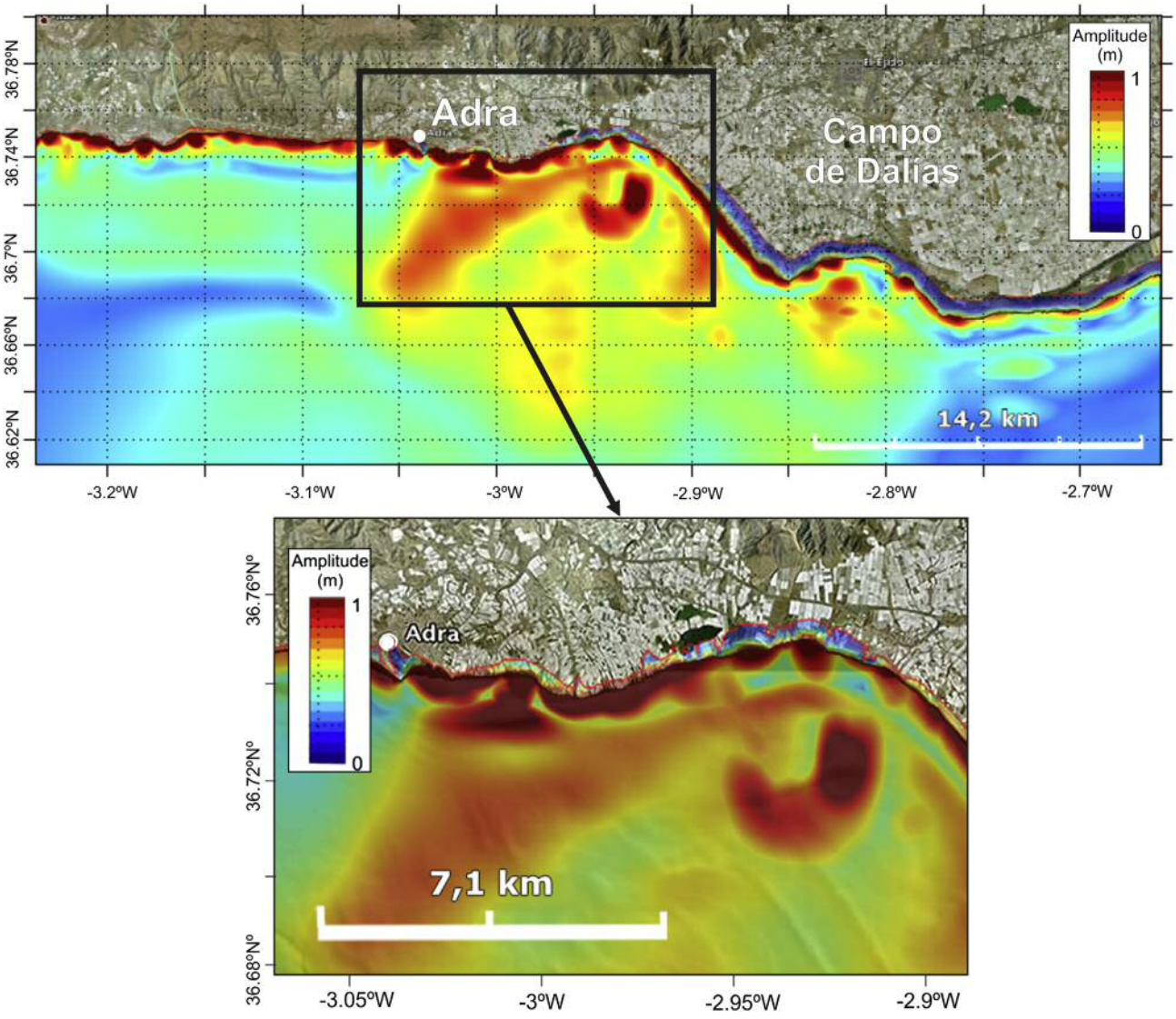

Fig. 17. Simulated maximal amplitude reached in the coastal area near Adra. Offshore the scale refers to maximal wave amplitude and onshore to inundation maximum depth.

Canyon-Fan. The HySEA numerical model simulates the submarine landslide triggering the tsunami and the water mass evolution, wave propagation, and the final penetration of the tsunami waves onto the coast, reproducing first and subsequent tsunami wave impacts by means of a single coupled numerical model. The numerical model allows us to analyse the influence of basin morphology on the propagation features of the tsunami, such as its shape and propagation patterns, speed or wave amplitude and, finally, its impact on the coastlines of South Iberia and North Africa. Seamounts in this basin are a key factor to controlling the tsunami waves. The extension of the flooded area and run-up heights are direct outputs of the numerical simulation. The numerical treatment of wet/dry fronts allows the inundation and run-up height to be efficiently quantified with no need of imposing any kind of coastal boundary conditions. The model considered can also be used as a prediction tool for the simulation of potential landslide-generated tsunamis. Monitoring of critical areas where submarine landslides are more probable and modelling their consequences so that appropriate mitigation strategies can be designed are areas of key scientific and socio-economic interests.

Supplementary data to this article can be found online at http://dx.doi.org/10.1016/j.margeo.2014.12.006.

Acknowledgements

This research has been partially supported by the Junta de Andalucía research project TESELA (P11-RNM7069), the Spanish Government Research projects HySEA2 (MTM2009-11923) and MONTERA (CTM2009-14157-C02) and Universidad de Málaga, Campus de Excelencia Internacional Andalucía Tech.

The Spanish Secretaría General de Pesca (Ministerio de Agricultura, Alimentación y Medio Ambiente) provided the bathymetric multibeam data. The multi-GPU computations were performed at the Laboratory of Numerical Methods (University of Málaga). We thank Sergio Ortega and Marc de la Asunción for performing the numerical simulations and providing us with some graphics. We would like to thank D. Arcas and C.B. Harbitz for their very useful comments and remarks on a previous version of this manuscript; they helped us to greatly improve the final form of this work. We would also like to acknowledge two anonymous

reviewers for their constructive reviews that substantially improved the quality of this paper. Thanks are also given to Christine Laurin for revising the English text.

References

Alonso, B., Ercilla, G., Estrada, F., Casas, D., García, M., Vázquez, J.T., Yenes, M., Farran, M., 2010. Quaternary mass-movements on the Almería margin and adjacent trough (Alboran Sea). Rapports. Commission Internationale pour L'Exploration Scientifique de la Mer Méditerranée 39, p. 4.

Alonso, B., Ercilla, G., Vázquez, J.T., Juan, C., Casas, D., Estrada, F., García, M., Farran, M., D'Acremont, E., Gorini, Ch., 2012. Caracterización morfo-sísmica de las inestabilidades sedimentarias del sector oriental del Mar de Alborán durante el Cuaternario (SO Mediterráneo). Geo-Temas 13, 557–560.

Alonso, B., Ercilla, G., García, M., Vázquez, J.T., Juan, C., Casas, D., Estrada, F., Alonso, B., Ercilla, G., García, M., Vázquez, J.T., Juan, C., Casas, D., Estrada, F., D'Acremont, E., Gorini, Ch., El Moumni, B., Farran, M., 2014. Quaternary mass-transport deposits on the North-Eastern Alboran Seamounts (SW Mediterranean Sea). 10.1007/978-3-319-00972-8-50). In: Krastel, S., et al. (Eds.), Submarine Mass Movements and Their Consequences. Springer Verlag Publishing, Berlin, pp. 561–570.

Álvarez-Gómez, J.A., Aniel-Quiroga, Í., González, M., Olabarrieta, M., Carreño, E., 2011a. Scenarios for earthquake-generated tsunamis on a complex tectonic area of diffuse deformation and low velocity: The Alboran Sea, Western Mediterranean. Marine Geology 284 (1–4), 55–73.

Álvarez-Gómez, J.A., Aniel-Quiroga, Í., González, M., Otero, L., 2011b. Tsunami hazard at the Western Mediterranean Spanish coast from seismic sources. Natural Hazards and Earth Systems Sciences 11, 227–240.

Ambraseys, N.N., 1981. The El-Asnam (Algeria) earthquake of 10 October 1980: conclusions drawn from a field study. American Journal of Engineering Geology 1414 (Part 2), 143–148.

Ballesteros, M., Rivera, J., Muñoz, A., Muñoz-Martín, A., Acosta, J., Carbó, A., Uchupi, E., 2008. Alboran Basin, southern Spain — part II: neogene tectonic implications for the orogenic float model. Marine and Petroleum Geology 25 (1), 75–101.

Bárcenas, P., 2002. Morfología submarina y evolución reciente del Banco de la Isla de Alborán. Tesis de Licenciatura. Universidad de Cádiz (481 pp).

Bárcenas, P., Vázquez, J.T., Díaz del Río, V., Fernández-Salas, L.M., 2004. Geomorfología del Banco de la Isla de Alborán. Geotemas 6 (2), 209–212.

Braga, J.C., Martín, J.M., Quesada, C., 2003. Pattern and average rates of late Neogene — recent uplift of the Betic Cordillera, SE Spain. Geomorphology 50, 3–26.

Buforn, E., Bexxeghoud, M., Udias, A., Pro, C., 2004. Seismic sources in the Iberia-African plate boundary and their tectonic implications. Pure and Applied Geophysics 161, 623–646.

Campos Romero, M.L., 1989. Sismicidad de la costa sudoccidental de España. Análisis y valoración geográfica de los posibles riesgos como consecuencia de los tsunamis de la zona. 2. Universidad Complutense de Madrid (515 + 219 pp.)

Casas, D., Ercilla, G., Yenes, M., Estrada, F., Alonso, B., García, M., Somoza, L., 2011. The Baraza Slide. Model and dynamics. Marine Geophysical Research 32 (1), 245–256.

Castro, M.J., Ferreiro, A.M., García-Rodríguez, J.A., González-Vida, J.M., Macías, J., Parés, C., Vázquez-Cendón, M.E., 2005. The numerical treatment of wet/dry fronts in shallow flows: application to one-layer and two-layer systems. Mathematical and Computer Modelling 3–4 (42), 419–439.

Castro, M.J., González-Vida, J.M., Parés, C., 2006. Numerical treatment of wet/dry fronts in shallow flows with a modified Roe scheme. Mathematical Models and Methods in Applied Sciences 16 (6), 897–931.

Castro, M.J., Chacón, T., Fernández-Nieto, E.D., González-Vida, J.M., Parés, C., 2008. Well-balanced finite volume schemes for 2D non-homogeneus hyperbolic systems. Applications to the dam break of Aznalcóllar. Computer Methods in Applied Mechanics and Engineering 197 (45), 3932–3950.

Castro, M.J., Fernández-Nieto, E.D., González-Vida, J.M., Parés, C., 2011a. Numerical treatment of the loss of hyperbolicity of the two-layer shallow-water system. Journal of Scientific Computing 1 (48), 16–40.

Castro, M.J., Ortega, S., de la Asunción, M., Mantas, J.M., Gallardo, J.M., 2011b. GPU computing for shallow water flows simulation based on finite volume schemes. Comptes Rendus Mecanique 339 (2–3), 165–184.

Castro, M.J., de la Asunción, M., Macías, J., Parés, C., Fernández-Nieto, E.D., González-Vida, J.M., Morales, T., 2012. In: Vázquez, E., Hidalgo, A., García, P., Cea, L. (Eds.), IFCP Riemann solver: Application to tsunami modelling using GPUs. CRC Press, pp. 237–244 (Chapter 5).

Cattaneo, A., Babonneau, N., Ratzov, G., Dan-Unterseh, G., Yelles, K., Bracene, R., Mercier de Lépinay, B., Boudiaf, A., Déverchère, J., 2012. Searching for the seafloor signature of the 21 May 2003 Boumerds earthquake offshore central Algeria. Natural Hazards and Earth Systems Sciences 12, 2159–2172.

COMCOT model. http://ceeserver.cee.cornell.edu/pll-group/ comcot.htm developed by Philip Liu's research group. Cornell Univ. USA.

Cordier, S., Le, M., Morales de Luna, T., 2011. Bedload transport in shallow water models: why splitting (may) fail, how hyperbolicity (can) help. Advances in Water Resources 8 (34), 980–989.

Dan, G., Sultan, N., Savoye, B., 2007. The 1979 Nice harbour catastrophe revisited: trigger mechanism inferred from geotechnical measurements and numerical modelling. Marine Geology 245, 40–64.

de la Asunción, M., Mantas, J.M., Castro, M.J., 2012. Evaluating the impact of cell renumbering of unstructured meshes on the performance of finite volume GPU solvers. 12th International Conference on Computational and Mathematical Methods in Science and Engineering (CMMSE 2012), La Manga (España), Julio 2012.

de la Asunción, M., Castro, M.J., Fernández-Nieto, E.D., Mantas, J.M., Ortega, S., González-Vida, J.M., 2013. Efficient GPU implementation of a two waves TVD-WAF method for the two-dimensional one layer shallow water system on structured meshes. Computers and Fluids 80, 441–452.

de Vicente, G., Cloetingh, S., Muñoz-Martín, A., Olaiz, A., Stich, D., Vegas, R., Galindo-Zaldívar, J., Fernández-Lozano, J., 2008. Inversion of moment tensor focal mechanisms for active stresses around the microcontinent Iberia: tectonic implications. Tectonics 27 (1). http://dx.doi.org/10.1029/2006TC002093 (art. no. TC1009, 22 pp.).

Dutykh, D., Katsaounis, Th., Mitsotakis, D., 2013. Finite volume methods for unidirectional dispersive wave models. International Journal for Numerical Methods in Fluids 71, 717–736.

El-Robrini, M., Genesseaux, M., Mauffret, A., 1985. Consequences of the El-Asnam earthquake: turbidity currents and slumps on the Algerian margin (Western Mediterranean). Geo-Marine Letters 5, 171–176.

Ercilla, G., Juan, C., Estrada, F., Casas, D., Alonso, B., García, M., Farran, M., Palomino, D., Vázquez, J.T., Llave, E., Hernández-Molina, F.J., Medialdea, T., Gorini, C., D'Acremont, E., El Moumni, B., Gensous, B., Tesson, M., Maldonado, A., Ammar, A., Contouriber, Montera Teams, 2012. Contourite sedimentation in the Alboran Sea: morphosedimentary characterization. Geo-Temas 13, 1809–1812 (CD anexo).

Fernández-Ibáñez, F., Soto, J.I., Zoback, M.D., Morales, J., 2007. Present-day stress field in the Gibraltar Arc (western Mediterranean). Journal of Geophysical Research, B: Solid Earth 112 (8). http://dx.doi.org/10.1029/2006JB004683 (art. no. B08404, 25 pp.).

Fernández-Nieto, E.D., Bouchut, F., Bresch, D., Castro, M.J., Mangeney, A., 2008. A new Savage–Hutter type model for submarine avalanches and generated tsunami. Journal of Computational Physics 227, 7720–7754.

Fernández-Nieto, E.D., Castro, M.J., Parés, C., 2011. On an intermediate field capturing Riemann solver based on a parabolic viscosity matrix for the two-layer shallow water system. Journal of Scientific Computing 48, 117–140.

Fine, I.V., Rabinovich, A.B., Bornhold, B.D., Thomson, R.E., Kulikov, E.A., 2005. The Grand Banks landslide-generated tsunami of November 18, 1929: preliminary analysis and numerical modeling. Marine Geology 215 (1Ð2), 45–57.

Gallardo, J.M., Parés, C., Castro, M.J., 2007. On a well-balanced high-order finite volume scheme for shallow water equations with topography and dry areas. Journal of Computational Physics 227, 574–601.

García, M., Alonso, B., Ercilla, G., Gràcia, E., 2006. The tributary valley systems of the Almeria Canyon (Alboran Sea, SW Mediterranean): sedimentary architecture. Marine Geology 226 (3–4), 207–223.

Giménez, J., Suriñach, E., Goula, X., 2000. Quantification of vertical movements in the Eastern Betics (Spain) by comparing levelling data. Tectonophysics 317, 237–258.

Glimsdal, S., Pedersen, G.K., Harbitz, C.B., Løvholt, F., 2013. Dispersion of tsunamis: does it really matter? Natural Hazards and Earth Systems Sciences 13, 1507–1526.

González, M., Medina, R., Olabarrieta, M., Otero, L., 2010. Tsunami hazard assessment in the Southern coast of Spain. Turkish Journal of Earth Sciences 19, 351–366.

González-Vida, J.M., Macías, J., Castro, M.J., de la Asunción, M., Sánchez-Linares, C., Ortega-Acosta, S., 2014. Modeling Lituya Bay landslide-generated mega-tsunami with a Savage–Hutter Shallow-Water coupled model. Contract report sent to NOAA. Paper in progress (Can be downloaded at https://www.researchgate.net/publication/265250065_Lituya_GJI?ev = prf_pub).

Gràcia, E., Pallàs, R., Soto, J.I., Comas, M., Moreno, X., Masana, E., Santanach, P., Diez, S., García, M., Dañobeitia, J., Bartolomé, R., Farrán, M., Gómez, M., Alpiste, M.J.R., Lastras, G., Wilmott, V., Perea, H., Blondel, P., Gómez, O., Bullock, L., Jacobs, C., Rouse, I., White, D., Whittle, S., Terrinha, P., Gafeira, J., Roque, C., 2006. Active faulting offshore SE Spain (Alboran Sea): Implications for earthquake hazard assessment in the Southern Iberian Margin. Earth and Planetary Science Letters 241 (3–4), 734–749.

Grilli, S.T., Harris, J.C., Tayebeh, S., Bakhsh, T., Masterlark, T.L., Kyriakopoulos, C., Kirby, J.T., Shi, F., 2012. Numerical simulation of the 2011 Tohoku tsunami based on a new transient FEM Co-seismic source: comparison to far- and near-field observations. Pure and Applied Geophysics 170 (6–8), 1333–1359. http://dx.doi.org/10.1007/s00024-012-0528-y.

EDANYA Group, 2015. Validation and verification of HySEA tsunami model In progress.

Harbitz, C.B., 1992. Model simulations of tsunamis generated by the Storegga slides. Marine Geology 105, 1–21.

Harbitz, C., Parker, G., Elverhøi, A., Marr, J.G., Mohrig, D., Harff, P.A., 2003. Hydroplaning of subaqueous debris flows and glide blocks: analytical solutions and discussion. Journal of Geophysical Research 108 (B7), 23–49. http://dx.doi.org/10.1029/2001JB001454.

Harbitz, C.B., Løvholt, F., Pedersen, G., Masson, D.G., 2006. Mechanisms of tsunami generation by submarine landslides: a short review. Norsk Geologisk Tidsskrift 86 (3), 255–264.

Harbitz, C.B., Løvholt, F., Bungum, H., 2014. Submarine landslide tsunamis: how extreme and how likely? Natural Hazards 72, 1341–1374.

Haugen, K.B., Løvholt, F., Harbitz, C.B., 2005. Fundamental mechanisms for tsunami generation by submarine flows in idealised geometries. Marine and Petroleum Geology 22, 209–217.

Heinrich, P.H., Piatanesi, A., Hébert, H., 2001. Numerical modelling of tsunami generation and propagation from submarine slumps: the 1998 Papua New Guinea event. Geophysical Journal International 145, 97–111. http://dx.doi.org/10.1111/j.1365-246X.2001.00336.x.

Hernández-Molina, F.J., Serra, N., Stow, D.A.V., Llave, E., Ercilla, G., Van Rooij, D., 2011. Along-slope oceanographic processes and sedimentary products around the Iberian margin. Geo-Marine Letters 31, 315Ð341. http://dx.doi.org/10.1007/s00367-011-0242-2.

Iglesias, O., Lastras, G., Canals, M., Olabarrieta, M., González, M., Aniel-Quiroga, I., Otero, L., Durán, R., Amblas, D., Casamor, J.L., Tahchi, E., Tinti, S., De Mol, B., 2012. The BIG'95

submarine landslide-generated tsunami; a numerical simulation. The Journal of Geology 120 (1), 31–48.
Jiang, L., Leblond, P.H., 1992. The coupling of a submarine slide and the surface waves which it generates. Journal of Geophysical Research 97 (C8), 12731–12744.
Kowalik, Z., Murty, T.S., 1993. Numerical modeling of ocean dynamics. World Scientific Pub (481 pp.).
Lastras, G., De Blasio, F.V., Canals, M., Elverhøi, A., 2005. Conceptual and numerical modeling of the Big'95 debris flow, western Mediterranean Sea. Journal of Sedimentary Research 75, 784–797.
Locat, J., Lee, H.J., 2002. Submarine landslides: advances and challenges. Canadian Geotechnical Journal 39, 193–212.
Løvholt, F., Harbitz, C.B., Haugen, K.B., 2005. A parametric study of tsunamis generated by submarine slides in the Ormen Lange/Storegga area off western Norway. Marine and Petroleum Geology 22, 219–231.
Macías, J., Fernández-Salas, L.M., González-Vida, J.M., Vázquez, J.T., Castro, M.J., Bárcenas, P., Díaz del Río, V., Morales, T., de la Asunción, M., Parés, C., 2012. Deslizamientos submarinos y tsunamis en el Mar de Alborán. Un ejemplo de modelización numérica. Temas de Oceanografía, IEO 978-84-95877-25-3 (187 pp).
Macías, J., Castro, M.J., González-Vida, J.M., Ortega, S., 2013. Non-linear shallow water models for coastal run-up simulations. EGU (2013).
Macías, J., González-Vida, J.M., Mercado, A., Ortega, S., Castro, M.J., 2015. Numerical simulation of LANTEX 2013 tsunami scenario with HySEA model. Impact assessment on Puerto Rico coasts In progress.
Maestro-González, A., Bárcenas, P., Vázquez, J.T., Díaz-del-Río, V., 2008. The role of basement inheritance faults in the recent fracture system of the inner shelf around Alboran Island, Western Mediterranean. Geo-Marine Letters 28 (1), 53–64.
Martínez-García, P., Comas, M., Soto, J.I., Lonergan, L., Pérez-Hernández, S., 2009. Deslizamientos submarinos recientes en la Cresta de Alborán (Mar de Alborán). Geogaceta 47, 89–92.
Martínez-García, P., Soto, J.I., Comas, M., 2011. Recent structures in the Alboran Ridges and Yusuf faults zones base on swath bathymetry and sub-bottom profiling: evidence of active tectonics. Geo-Marine Letters 31, 19–36.
Martínez-García, P., Comas, M., Soto, J.I., Lonergan, L., Watts, A.B., 2013. Strike-slip tectonics and basin inversión in the Western Mediterranean: the Post-Messinian evolution of the Alboran Sea. Basin Research 25, 361–387.
Masson, D.G., Harbitz, C.B., Wynn, R.B., Pedersen, G., Løvholt, F., 2006. Submarine landslides: processes, triggers and hazard prediction. Philosophical Transactions of the Royal Society A: Mathematical, Physical and Engineering Sciences 364, 2009–2039.
Papadopoulos, G.A., Gràcia, E., Urgeles, R., Sallares, V., De Martini, P.M., Pantosti, D., González, M., Yalciner, A.C., Mascle, J., Sakellariou, D., Salamon, A., Tinti, S., Karastathis, V., Fokaefs, A., Camerlenghi, A., Novikova, T., Papageorgiou, A., 2014. Historical and pre-historical tsunamis in the Mediterranean and its connected seas: geological signatures, generation mechanisms and coastal impacts. Marine Geology 354, 81–109.
Platt, J.P., Whitehouse, M.J., Kelley, S.P., Carter, A., Hollick, L., 2003. Simultaneous extensional exhumation across the Alboran basin: implications for the causes of late-orogenic extension. Geology 31, 259–262.
Reicherter, K., Becker-Heidmann, P., 2009. Tsunami deposits in the western Mediterranean: remains of the 1522 Almería earthquake? Geological Society Special Publication 316, 217–235.
Sahal, A., Roger, J., Allgeyer, S., Lemaire, B., Hébert, H., Schindelé, F., Lavigne, F., 2009. The tsunami triggered by the 21 May 2003 Boumerds-Zemmouri (Algeria) earthquake: field investigations on the French Mediterranean coast and tsunami modelling. Natural Hazards and Earth Systems Sciences 9, 1823–1834.
Satake, K., 1995. Linear and nonlinear computations of the 1992 Nicaragua earthquake tsunami. Pure and Applied Geophysics 144, 455–470.
Savage, S.B., Hutter, K., 1989. The motion of a finite mass of granular material down a rough incline. Journal of Fluid Mechanics 199, 177–215.
Shigihara, Y., Goto, D., Imamura, F., Kitamura, Y., Matsubara, T., Takaoka, K., Ban, K., 2006. Hydraulic and numerical study on the generation of a subaqueous landslide-induced tsunami along the coast. Natural Hazards 39, 159Ð177.
Skvortsov, A., 2002. Numerical simulation of landslide generated tsunamis with application to the 1975 failure in Kitimat Arm, British Columbia, Canada. PhD. Thesis. School of Earth and Ocean Sciences,University of Victoria, British Columbia.
Soloviev, S.L., Campos-Romero, M.L., Plink, N.L., 1992. Orleansville tsunami of 1954 and El Asnam tsunami of 1980 in the Alboran Sea (Southwestern Mediterranean Sea). Izvestiya, Earth Physics 28 (9), 739–760.
Soloviev, S.L., Go, C.N., Kim, K.S., Solovieva, O.N., Shchetnikov, N.A., 1997. Tsunamis in the Mediterranean Sea; 2000 B.C.–1991 A.D. Moscow: Nauka (139p [in Russian]).
Soloviev, S.L., Solovieva, O.N., Go, C.N., Kim, K.S., Shchetnikov, N.A., 2000. Tsunamis in the Mediterranean Sea 2000 B.C.–2000 A.D. Advances in Natural and Technological Hazards Research. 13. Kluwer Academic Publishers, Dordrecht (237 pp.).
Stich, D., Batlló, J., Morales, J., Macià, R., Dineva, S., 2003. Source parameters of the Mw = 6.1 1910 Adra earthquake (southern Spain). Geophysical Journal International 155, 539–546.
Stich, D., Mancilla, F.-L., Baumont, D., Morales, J., 2005. Source analysis of the Mw 6.3 2004 Al Hoceima earthquake (Morocco) using regional apparent source time functions. Journal of Geophysical Research 110 (6), 1–13.
Stich, D., Serpelloni, E., Mancilla, F.-L., Morales, J., 2006. Kinematics of the Iberia–Maghreb plate contact from seismic moment tensors and GPS observations. Tectonophysics 426, 295–317.
Stich, D., Martin, R., Morales, J., 2010. Moment tensor inversion for Iberia–Maghreb earthquakes 2005–2008. Tectonophysics 483, 390–398.
Tappin, D.R., 2010. Submarine mass failure as tsunami sources: their climate control. Philosophical Transactions of the Royal Society A: Mathematical, Physical and Engineering Sciences 368, 2417–2434.
Tinti, S., Pagnoni, G., Zaniboni, F., 2006. The landslides and tsunamis of the 30th of December 2002 in Stromboli analysed through numerical simulations. Bulletin of Volcanology 68 (5), 462–479.
Tinti, S., Chiocci, F.L., Zaniboni, F., Pagnoni, G., de Alteriis, G., 2011. Numerical simulation of the tsunami generated by a past catastrophic landslide on the volcanic island of Ischia, Italy. Marine Geophysical Research 32, 287–297.
Titov, V.V., González, F.I., 1997. Implementation and testing of the Method of Splitting Tsunami (MOST) model. NOAA Technical Memorandum ERL PMEL-112 (11 pp.).
Vázquez, J.T., Vegas, R., 2000. Acomodación de la convergencia entre África y la Península Ibérica, Golfo de Cádiz y Mar de Alborán, a partir del análisis de terremotos. Geogaceta 27, 171–174.
Vázquez, J.T., Vegas, R., Medialdea, T., 2008. Estructuras recientes de deformación en el margen continental del Mar de Alborán (Sector Benalmádena-Adra). Geo-Temas 10 (SO7029), 595–598.
Vázquez, J.T., Bárcenas, P., Palomino, D., Alonso, B., Ercilla, B., Díaz del Río, V., López-González, N., Fernández-Salas, L.M., Sayago-Gil, M., 2010. Sedimentary instabilities along the soughtern slope of the Alboran Ridge (SW Meditterranean). Rapports. Commission Internationale pour L'Exploration Scientifique de la Mer Méditerranée 39, 76.
Vázquez, J.T., Alonso, B., MONTERA team, 2012. Informe Científico-Técnico de la Campaña Oceanográfica MONTERA 0412. Repositorio IEO (URI: http://hdl.handle.net/10508/994. Documento GEMAR 2012-03, 1-34, anexos).
Vázquez, J.T., Alonso, B., Palomino, D., Ercilla, G., Juan, C., Bárcenas, P., Casas, D., Estrada, F., López-González, N., Fernández-Puga, M.C., García, M., Roque, C., El Moumni, B., d'Acremont, E., Díaz del Río, V., Fernández-Salas, L.M., Gorini, Ch., Montera Team, 2013. Mass movement deposits and tectonics relation as a main factor to control the stratigraphical architecture of the South Alboran Basin (Alboran Sea, Western Mediterranean). Vth Regional Committee on Atlantic Neogene Stratigraphy. Atlantic Neogene Ð Two Decades of Study. Huelva (Españapp. 46–47.
Vázquez, J.T., Alonso, B., Fernández-Puga, M.C., Gómez-Ballesteros, M., Iglesias, J., Palomino, D., Roque, C., Ercilla, G., Díaz-del-Río, V., 2014. Seamounts along the Iberian Continental Margins: a key morphological feature. Boletín Geológico Minero 125 49 pp.
Vegas, R., Medialdea, T., Vázquez, J.T., 2008. Sobre la naturaleza del límite de placas actual entre la Península Ibérica y el norte de África. Geo-Temas 10 (SP1O10), 1535–1538.
Watts, P., Grilli, S.T., Kirby, J.T., Fryer, G.J., Tappin, R., 2003. Landslide tsunami case studies using a Boussinesq model and a fully nonlinear tsunami generation model. Natural Hazards and Earth System Sciences 3, 391–402.
Yielding, G., Jackson, J., King, G., Sinvhal, H., Vita-Finzi, C., Wood, R., 1981. Relations between surface deformation, fault geometry, seismicity and rupture characteristics during the El-Asnam (Algeria) earthquake of 10 de October 1980. Earth and Planetary Science Letters 56, 287–304.